Cell Reports

Article

Identification of fibrocyte cluster in tumors reveals the role in antitumor immunity by PD-L1 blockade

Graphical abstract

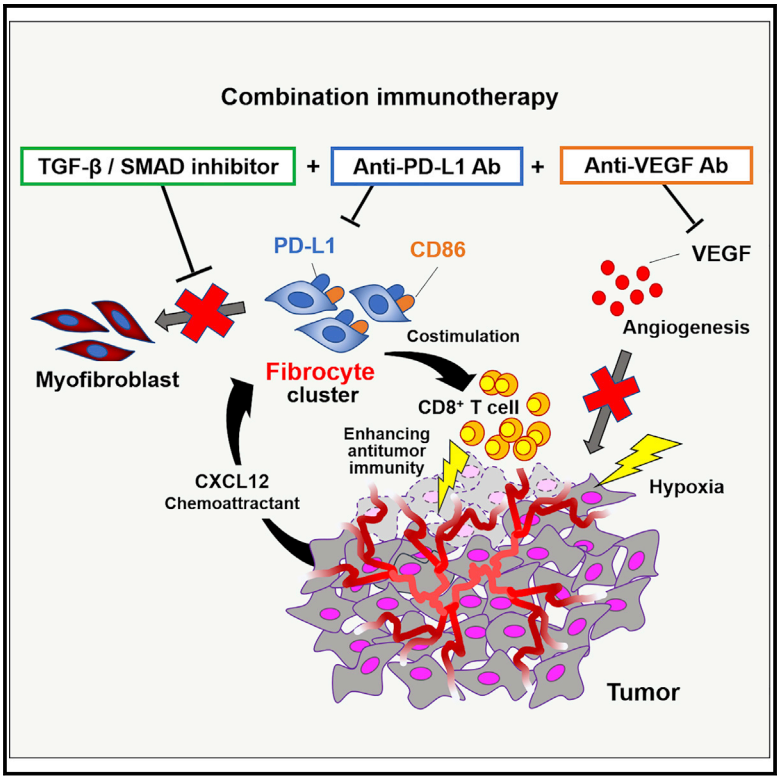

Authors

Atsushi Mitsuhashi, Kazuya Koyama, Hirokazu Ogino, ..., Hiromitsu Takizawa, Tsutomu Shinohara, Yasuhiko Nishioka

Correspondence

yasuhiko@tokushima-u.ac.jp

In brief

Mitsuhashi et al. identify the distinct population of fibrocytes in the tumors treated with angiogenesis inhibitor, and they reveal their T cell-costimulatory capacities. These findings highlighted the control of tumor-infiltrating fibrocytes as a promising strategy for the advancement of combination immunotherapy.

Highlights

- Single-cell RNA sequencing identifies a distinct fibrocyte cluster in tumor tissue
- Tumor-infiltrating fibrocytes enhance antitumor effects of PD-L1 blockade via CD86
- Fibrocytes sorted from tumors show T cell costimulation enhanced by PD-L1 blockade
- SMAD inhibitor augments antitumor immunity by regulating fibrocyte differentiation

Mitsuhashi et al., 2023, Cell Reports *42*, 112162
March 28, 2023
https://doi.org/10.1016/j.celrep.2023.112162

CellPress

Cell Reports

CellPress
OPEN ACCESS

Article

Identification of fibrocyte cluster in tumors reveals the role in antitumor immunity by PD-L1 blockade

Atsushi Mitsuhashi,[1] Kazuya Koyama,[1] Hirokazu Ogino,[1] Tania Afroj,[1] Na Thi Nguyen,[1] Hiroto Yoneda,[1] Kenji Otsuka,[1] Masamichi Sugimoto,[2] Osamu Kondoh,[2] Hiroshi Nokihara,[1] Masaki Hanibuchi,[1,3] Hiromitsu Takizawa,[4] Tsutomu Shinohara,[5] and Yasuhiko Nishioka[1,6,7,*]

[1]Department of Respiratory Medicine and Rheumatology, Graduate School of Biomedical Sciences, Tokushima University, Tokushima 770-8503, Japan

[2]Product Research Department, Kamakura Research Laboratories, Chugai Pharmaceutical Co., Ltd, Kamakura 247-8530, Japan

[3]Department of Community Medicine for Respirology, Hematology and Metabolism, Graduate School of Biomedical Sciences, Tokushima University, Tokushima 770-8503, Japan

[4]Department of Thoracic and Endocrine Surgery and Oncology, Graduate School of Biomedical Sciences, Tokushima University, Tokushima 770-8503, Japan

[5]Department of Community Medicine for Respirology, Graduate School of Biomedical Sciences, Tokushima University, Tokushima 770-8503, Japan

[6]Department of Community Medicine for Rheumatology, Graduate School of Biomedical Sciences, Tokushima University, Tokushima 770-8503, Japan

[7]Lead contact

*Correspondence: yasuhiko@tokushima-u.ac.jp

https://doi.org/10.1016/j.celrep.2023.112162

SUMMARY

Recent clinical trials revealed that immune checkpoint inhibitors and antiangiogenic reagent combination therapy improved the prognosis of various cancers. We investigated the roles of fibrocytes, collagen-producing monocyte-derived cells, in combination immunotherapy. Anti-VEGF (vascular endothelial growth factor) antibody increases tumor-infiltrating fibrocytes and enhances the antitumor effects of anti-PD-L1 (programmed death ligand 1) antibody *in vivo*. Single-cell RNA sequencing of tumor-infiltrating $CD45^+$ cells identifies a distinct "fibrocyte cluster" from "macrophage clusters" *in vivo* and in lung adenocarcinoma patients. A sub-clustering analysis reveals a fibrocyte sub-cluster that highly expresses co-stimulatory molecules. $CD8^+$ T cell-costimulatory activity of tumor-infiltrating $CD45^+CD34^+$ fibrocytes is enhanced by anti-PD-L1 antibody. Peritumoral implantation of fibrocytes enhances the antitumor effect of PD-L1 blockade *in vivo*; $CD86^{-/-}$ fibrocytes do not. Tumor-infiltrating fibrocytes acquire myofibroblast-like phenotypes through transforming growth factor β (TGF-β)/small mothers against decapentaplegic (SMAD) signaling. Thus, TGF-βR/SMAD inhibitor enhances the antitumor effects of dual VEGF and PD-L1 blockade by regulating fibrocyte differentiation. Fibrocytes are highlighted as regulators of the response to programmed death 1 (PD-1)/PD-L1 blockade.

INTRODUCTION

Immune checkpoint inhibitors (ICIs), including monoclonal antibodies targeting programmed death 1 (PD-1) and its ligand, programmed death ligand 1 (PD-L1), provide clinical benefits in different malignancies.[1,2] Recently, various combination of ICIs with other modalities, including cytotoxic agents, radiotherapy, and molecular targeted agents, have been explored to mediate synergistic antitumor effects in murine models and humans.[3,4] Notably, angiogenesis inhibitors targeting vascular endothelial growth factor (VEGF) and VEGF receptor (VEGFR) have been expected to enhance the antitumor effects of ICIs.[4–6] In fact, recent data from phase III clinical trials demonstrated the superiority of combination therapy with anti-PD-L1 antibody (atezolizumab) and anti-VEGF antibody (bevacizumab) in non-squamous non-small cell lung cancer (NSCLC), metastatic renal cell carcinoma, and hepatocellular carcinoma.[7–9]

Several studies have reported the roles of VEGF in tumor immunity.[3,10,11] VEGF is known to recruit regulatory T cells (T_{reg}s) and myeloid-derived suppressor cells (MDSCs) to inhibit the maturation of dendritic cells (DCs) and to directly suppress effector T cell activation.[10,11] Given these immunosuppressive functions of VEGF, blockade of VEGF/VEGFR signaling has drawn attention for its potential to reinforce the antitumor immunity. However, the immunological background showing additive or synergistic effects of combinations of ICIs and antiangiogenic agents remains unclear.

Fibrocytes are bone marrow-derived cells that have the phenotypes of both fibroblasts and macrophages.[12] Based on the

extracellular matrix (ECM)-producing and pro-inflammatory abilities, fibrocytes have long been proposed to contribute to the pathogenesis of fibrotic diseases, including pulmonary fibrosis, liver fibrosis, and cardiovascular disease.[12–14] Furthermore, we showed that fibrocytes promote tumor progression via the induction of cancer stem cell-like properties[15] and mediate acquired resistance to anti-VEGF therapy.[16] The mechanistic study indicated that VEGF blockade enhances tumor-derived CXCL12 production and recruits fibrocytes into tumors, where they produce an alternative angiogenic molecule: fibroblast growth factor 2.

Fibrocytes have also been demonstrated to have the features of antigen-presenting cells (APCs).[12,17] We recently revealed that fibrocytes derived from human peripheral blood and mouse lungs expressed costimulatory molecules ($CD80^{low}$, $CD86^{high}$) and coinhibitory molecule ($PD\text{-}L1^{high}$) and induced $CD8^+$ T cell proliferation via cross-presentation *in vitro*.[18] Furthermore, anti-PD-L1 antibody enhanced the antigen-presenting ability of fibrocytes. Based on these results, we hypothesized that tumor-infiltrating fibrocytes have the potential to enhance the antitumor effects of PD-1/PD-L1 blockade, especially in fibrocyte-rich tumors, such as in bevacizumab-treated cases. However, the characteristics and function of fibrocytes in tumors have not been analyzed because living fibrocytes are difficult to harvest because of the lack of a specific cell surface marker.

In the present study, we demonstrate "fibrocyte clusters" in tumors by performing single-cell RNA sequencing (scRNA-seq) of tumor-infiltrating $CD45^+$ hematopoietic cells in a syngeneic mouse model treated with VEGF blockade and lung adenocarcinoma patients. After analyzing the gene expression and differentiation of fibrocyte clusters, we isolated tumor-infiltrating fibrocytes as living cells and showed their T cell-costimulatory function and potential synergistic effects of PD-L1 antibody and anti-VEGF antibody.

RESULTS

Combination therapy with PD-L1 blockade and VEGF blockade showed synergistic effects in mouse models

To investigate the efficacy of anti-VEGF antibody in tumor angiogenesis, we subcutaneously injected syngeneic mice with mouse mesothelioma cell line AB1-influenza haemagglutinin gene (HA). Seven days after tumor injection, low-dose (0.5 mg/kg) or high-dose (5 mg/kg) anti-VEGF antibody was administered twice a week for 2 weeks. Low-dose anti-VEGF antibody failed to suppress tumor progression, whereas high-dose anti-VEGF antibody significantly inhibited tumor growth (Figure 1A). In contrast, both low-dose and high-dose anti-VEGF antibody suppressed tumor angiogenesis (Figure 1B). To evaluate the efficacy of combination blockade of PD-L1 and VEGF, we administered low-dose (0.5 mg/kg) anti-PD-L1 antibody and anti-VEGF antibody *in vivo* from day 7 (combination treatment schedule). Combination therapy with PD-L1 and VEGF blockade showed superior antitumor effects to monotherapy (Figure 1C) (anti-VEGF antibody versus combination, $p = 0.014$; anti-PD-L1 antibody versus combination, $p = 0.035$; day 21 tumor volume). Furthermore, in tumors treated with combination therapy, tumor-infiltrating $CD8^+$ T cells were increased more than 5-fold in comparison with the control group (Figure 1D). The antitumor effect of combination blockade of VEGF and PD-1 was also confirmed in AB1-HA-bearing mice (Figure 1E). Next, we investigated whether anti-VEGF antibody pretreatment could similarly generate synergistic antitumor effects to anti-PD-L1 antibody treatment, irrespective of the delayed administration, in order to confirm the importance of changes of the tumor microenvironment, including fibrocyte accumulation, induced by anti-VEGF antibody, which we reported previously.[16] As expected, pretreatment (from day 7) with low-dose anti-VEGF antibody was sufficient to show the synergistic antitumor effects of combination therapy with delayed (from day 14) anti-PD-L1 antibody treatment (sequential treatment schedule) (Figures 1F and 1G). Notably, sequential treatment showed similar antitumor effects to combination treatment. These findings imply the significance, and further analyses are required to investigate modification of the tumor microenvironment by anti-VEGF antibody in tumor immunotherapy with PD-1/PD-L1 antibodies.

scRNA-seq identifies fibrocyte clusters as novel tumor-related immune cells recruited by VEGF blockade

To analyze modification of the tumor microenvironment by VEGF blockade, we performed scRNA-seq of $CD45^+$ tumor-infiltrating immune cells from AB1-HA tumor tissues treated with control IgG (11,567 cells sequenced) or anti-VEGF antibody (8,704 cells sequenced). All 20,271 $CD45^+$ cells were clustered into cell-type classifications annotated with canonical marker gene expression levels using the Seurat package (Figures 2A–2C). We identified a distinct cluster of $CD45^+$ and $collagen1a1^+$ cells as tumor-infiltrating fibrocytes. Fibrocytes also displayed the expression of fibroblast activation-related genes, including SPARC and EGR1 (Figure 2B). The population clustered as fibrocytes also expressed known fibrocyte markers (e.g., S100A4, TM4SF1, and CD11b) (Figure 2D). In contrast, tumor-infiltrating fibrocytes expressed, to a lesser extent, other immune cell markers for macrophages (Cd68, Adgre1, Lyz2), DCs (Ly75), and granulocytes (Csf3r). The cluster analysis showed that fibrocyte clusters were indisputably independent from large macrophage clusters and had gene expression characteristics, although the broad and unseparated distribution of classical subset markers of macrophage clusters was observed, even in the case of M1- or M2-macrophage markers (Figures 2D and S1).

Analyzing VEGF blockade-induced changes in the subpopulation of tumor-infiltrating $CD45^+$ cells, we found that M1-like macrophages, granulocytes, and fibrocytes nearly doubled in tumor tissues treated with anti-VEGF antibody (Figures 2E and 2F). To confirm fibrocyte accumulation, we performed an immunohistochemical analysis of tumor-infiltrating fibrocytes ($Collagen1a1^+$ $CD45^+$) in AB1-HA tumor tissue (Figure 2G). VEGF blockade increased the tumor-infiltrating fibrocytes in a dose-dependent manner. The antitumor and antiangiogenic effects of VEGF blockade were also confirmed in mouse lung cancer cell line Lewis lung carcinoma (LLC)-bearing mice (Figures S2A and S2B). Dual blockade of VEGF and PD-L1 suppressed the tumor progression and increased the tumor-infiltrating $CD8^+$ T cells in LLC-bearing mice (Figures S2C and S2D). Anti-VEGF antibody also increased the tumor-infiltrating fibrocytes in LLC-bearing mice (Figure S2E). Because MDSCs and T_{reg}s are also known

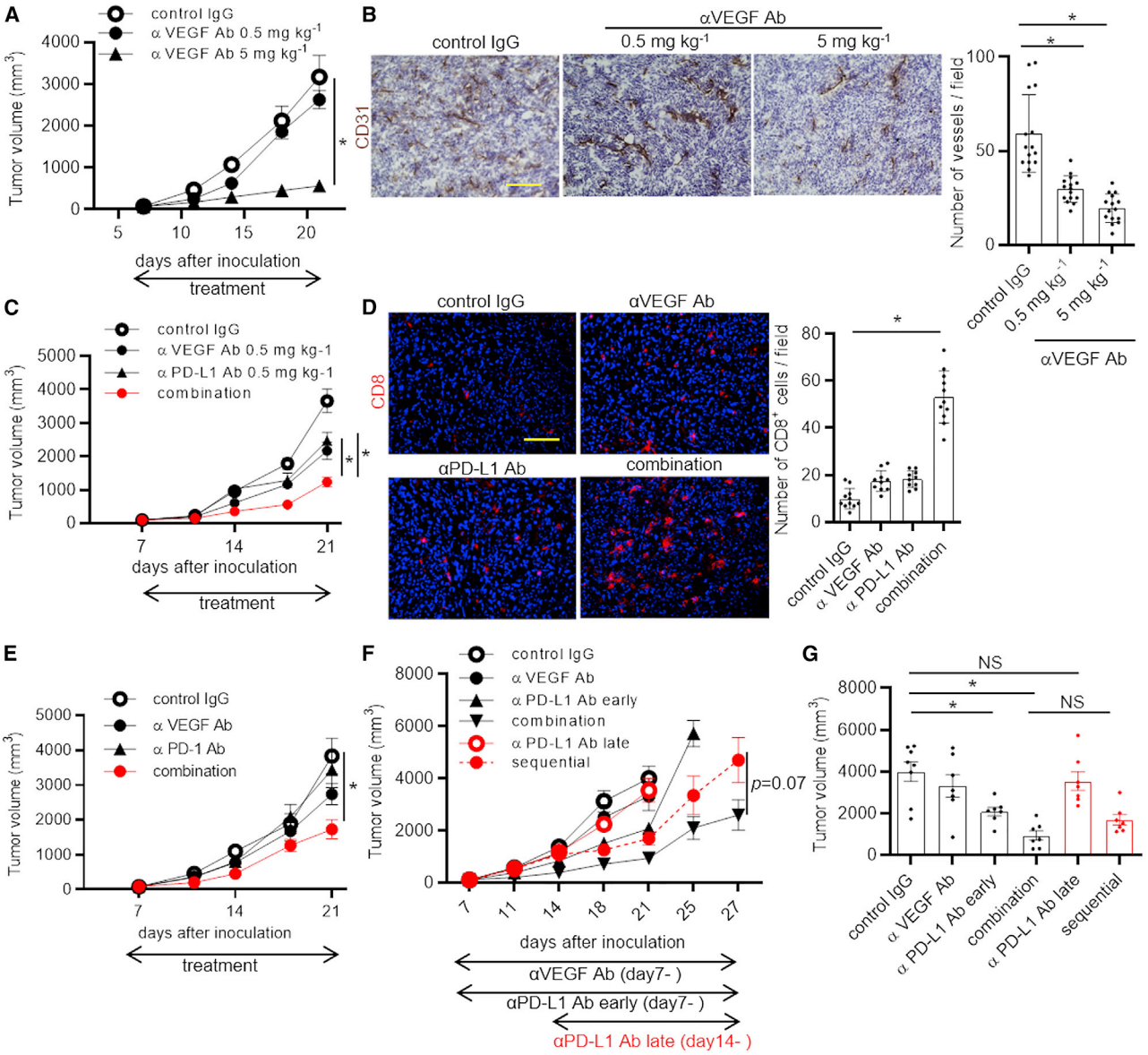

Figure 1. Combination therapy with dual PD-L1 and VEGF blockade shows synergistic antitumor effects *in vivo*

(A) The evaluation of the tumor volume of AB1-HA tumor-bearing mice treated with anti-VEGF antibody (αVEGF Ab) from 7 days after tumor cell injection (n = 7 per group). *p < 0.05 by one-way ANOVA.

(B) Representative images of sections from AB1-HA tumors stained for CD31 and the quantitative evaluation of the number of vessels per field (n = 15 field per group). Tumors were harvested on day 21 from the control IgG and αVEGF Ab-treated groups. Scale bar, 200 μm. *p < 0.05 by one-way ANOVA.

(C) The evaluation of the tumor volume of AB1-HA-bearing mice treated with low-dose αVEGF Ab and/or αPD-L1 Ab from 7 days after tumor cell injection (n = 7 per group). *p < 0.05 by one-way ANOVA.

(D) Representative images and quantitative evaluation of sections from AB1-HA tumors stained for CD8a (n = 15 field per group). The tumors were harvested at day 21 from each group in (C). Scale bar, 200 μm. *p < 0.05 by one-way ANOVA.

(E) The evaluation of the tumor volume of AB1-HA-bearing mice treated with low-dose αVEGF Ab (0.5 mg/kg) and/or αPD-1 Ab (200 μg per mouse) twice a week from 7 days after tumor cell injection (n = 7 per group). *p < 0.05 by one-way ANOVA.

(F) The evaluation of the tumor volume of AB1-HA-bearing mice treated with low-dose αVEGF Ab and/or αPD-L1 Ab from 7 (early) or 14 (late) days after tumor cell injection (n = 7 per group). *p < 0.05 by one-way ANOVA.

(G) The tumor volume of each group at day 21 in (E). *p < 0.05 by one-way ANOVA. The evaluations of immunohistochemical analysis are shown as the mean ± SD. The other data are shown as the mean ± SEM.

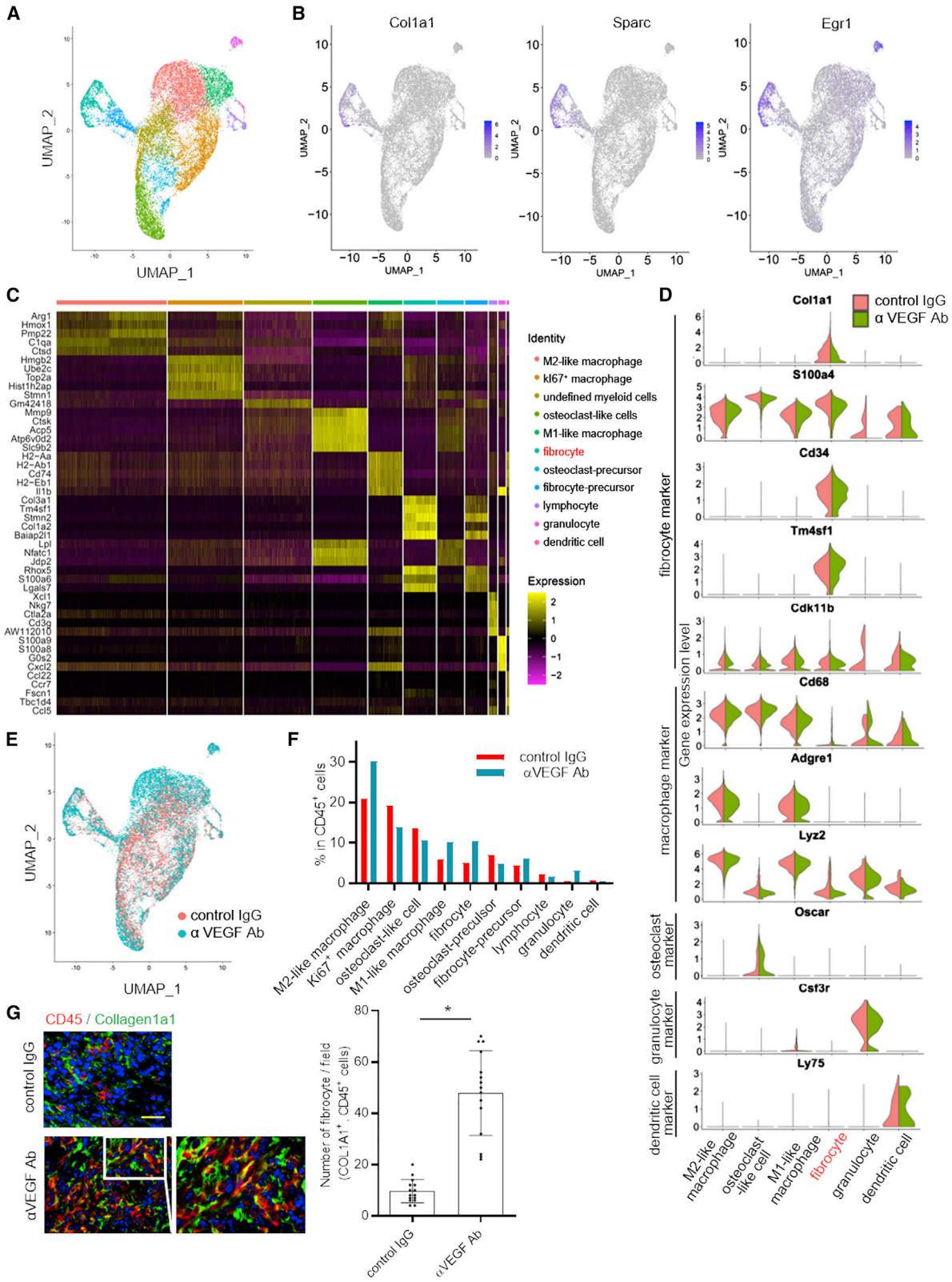

(legend on next page)

as immune suppressor lineages that are regulated by VEGF, we investigated the immunohistochemical analysis of their markers (Gr-1 and Foxp3) in AB1-HA tumor tissue (Figure S3), because both cells were minor populations and not detected as a cluster in our scRNA-seq data. Anti-VEGF antibody decreased the tumor-infiltrating MDCSs, whereas the number of T_{reg}s was not affected by either treatment.

scRNA-seq identifies tumor-infiltrating fibrocyte in lung adenocarcinoma cases

We also performed scRNA-seq of 38,145 $CD45^+$ tumor-infiltrating immune cells in resected tumor tissue from four lung adenocarcinoma patients (Figures S4A–S4C). We identified a distinct cluster of collagen-expressing $CD45^+$ cells as tumor-infiltrating fibrocytes in clinical cases (Figure S4D). Tumor-infiltrating fibrocytes in clinical lung adenocarcinoma expressed common markers (e.g., SPARC and TM4SF1) as fibrocytes identified in a preclinical model (Figures 2D and S4D). The frequency of tumor-infiltrating fibrocytes was 0.30%–2.49% in $CD45^+$ cells isolated from resected lung adenocarcinoma tissue (Figure S4A). Our previous reports also have shown the increase of tumor-infiltrating $FSP\text{-}1^+CD45^+$ fibrocytes in immunohistochemical analysis of tumor tissue from lung carcinoma patients who received neoadjuvant chemotherapy, including anti-VEGF blockade.[16] Besides, the number of tumor-infiltrating fibrocytes was lower in untreated tissue. Considering the results of scRNA-seq in untreated AB1-HA tumor (Figure 2F) and immunohistochemical analysis of human lung adenocarcinoma, we considered that the frequency of human tumor-infiltrating fibrocytes identified in the present scRNA-seq analysis was appropriate.

Subset clustering revealed a novel sub-population of fibrocytes possessing immune-modulating features

We next investigated the immune-modulating properties of tumor-infiltrating fibrocytes in more detail. The cluster of tumor-infiltrating fibrocytes identified in scRNA-seq expressed several immune-related molecules; however, the overall expression levels appeared lower than other APCs (e.g., macrophages and DCs) (Figure S1). Based on these findings, we assumed the existence of sub-populations among tumor-infiltrating fibrocytes that were specialized in tumor immunity. To examine their features, we performed a re-clustering analysis of tumor-infiltrating fibrocytes. Sub-clustering and a Gene Ontology (GO) analysis of fibrocytes revealed five sub-clusters, including fibroblastic (FC1), proliferating (FC2), and immune-related (FC3) populations (Figures 3A–3C). Among them, VEGF blockade increased FC1 and FC3, as well as the sub-cluster of fibrocytes exposed to hypoxia (FC0). Several studies revealed the potential of bone marrow-derived fibrocytes to differentiate into fibroblasts/myofibroblasts in various organs.[12,13,19] We considered that the increase of FC1 and FC3 reflected the differentiation process of recruited fibrocytes in tumor tissue. We therefore examined the gene expression levels of costimulatory molecules (CD80, CD86), MHC class II (H2-Aa, H2-Ab1), and immune checkpoint molecules (Cd274, Pdcdlg2) in each sub-cluster (Figure 3D). Interestingly, FC3 expressed high levels of CD86, but not CD80, MHC class II, and PD-L1, but not PD-L2, whereas FC2 ($Ki67^+$ proliferating fibrocytes) slightly expressed CD80 and MHC class II.

Even though each fibrocyte sub-cluster expressed ECM-associated genes (collagens and regulators of ECM), FC1 showed properties that were particularly close to fibroblasts (Figures 3D and S5). FC1 also expressed FGF2, which induced acquired resistance to VEGF blockade[16] (Figure S5). Thus, FC1 could have the potential to partially contribute to tumor progression as shown previously.[15,16] In contrast, FC3 may play a central role in tumor immunity as immune-related fibrocytes.

Fibrocytes enhanced antitumor effects of PD-1/PD-L1 blockade *in vivo*

To examine whether tumor-infiltrating fibrocytes contribute to the antitumor effects of PD-L1 blockade, we performed combination therapy with an anti-PD-L1 antibody and implantation of fibrocytes into AB1-HA tumors (Figure 4A). Mouse fibrocytes were isolated from lung tissue through 1-week culture in fibronectin-coated dishes and selection of $CD45^+$ cells.[16,18] As described previously, both lung fibrocyte and tumor-derived fibrocyte enhanced the T cell proliferation *in vitro*. Our previous study revealed that PD-L1 blockade augmented the co-stimulatory capacity of tumor-derived fibrocytes and lung-derived fibrocytes.[18] We routinely confirmed that mouse lung-derived fibrocytes express PD-L1 and CD86. Peritumoral implantation of mouse lung fibrocytes enhanced the antitumor effects of anti-PD-L1 antibody (Figure 4B) (control IgG versus anti-PD-L1 antibody; $p = 0.246$, control IgG versus combination; $p = 0.008$, day 21 tumor volume). Furthermore, mouse fibrocyte implantation combined with anti-PD-L1 antibody increased tumor-infiltrating $CD8^+$ T cells >3-fold in comparison with anti-PD-L1 antibody monotherapy (Figure 4C). Mouse lung fibrocytes also potentiated the antitumor effects of anti-PD-1 antibody *in vivo*

Figure 2. Tumor-infiltrating fibrocyte was identified as the distinct cluster enriched in immune-related and fibrotic molecules

(A) Uniform manifold approximation and projection (UMAP) plots of single-cell RNA-seq (scRNA-seq) data generated from $CD45^+$ cells in AB1-HA tumor tissue. Data are representative of two experiments with similar results.

(B) UMAP plots of selected fibrocyte markers from a merged condition.

(C) An expression heatmap of the top five differentially expressed genes in each cluster.

(D) Violin plots of selected genes in each myeloid cell, including macrophages, osteoclast-like cells, granulocytes, dendritic cells, and fibrocytes. The normalized expression levels were compared between mice treated with isotype control and mice treated with αVEGF Ab.

(E) Superimposed UMAP plot projections of scRNA-seq data from tumor-infiltrating $CD45^+$ cells in AB1-HA-bearing mice treated with isotype control and αVEGF Ab.

(F) Cluster proportions in tumor-infiltrating $CD45^+$ cells.

(G) Double staining of collagen1a1 and CD45 in tumors from mice treated with or without αVEGF Ab (the mice studied in Figure 1A; n = 15 field per group). Scale bar, 50 μm. The number of double-positive cells in the tumors was evaluated in each group. *$p < 0.05$ by one-way ANOVA.

The data are shown as the mean ± SD. See also Figures S1–S4.

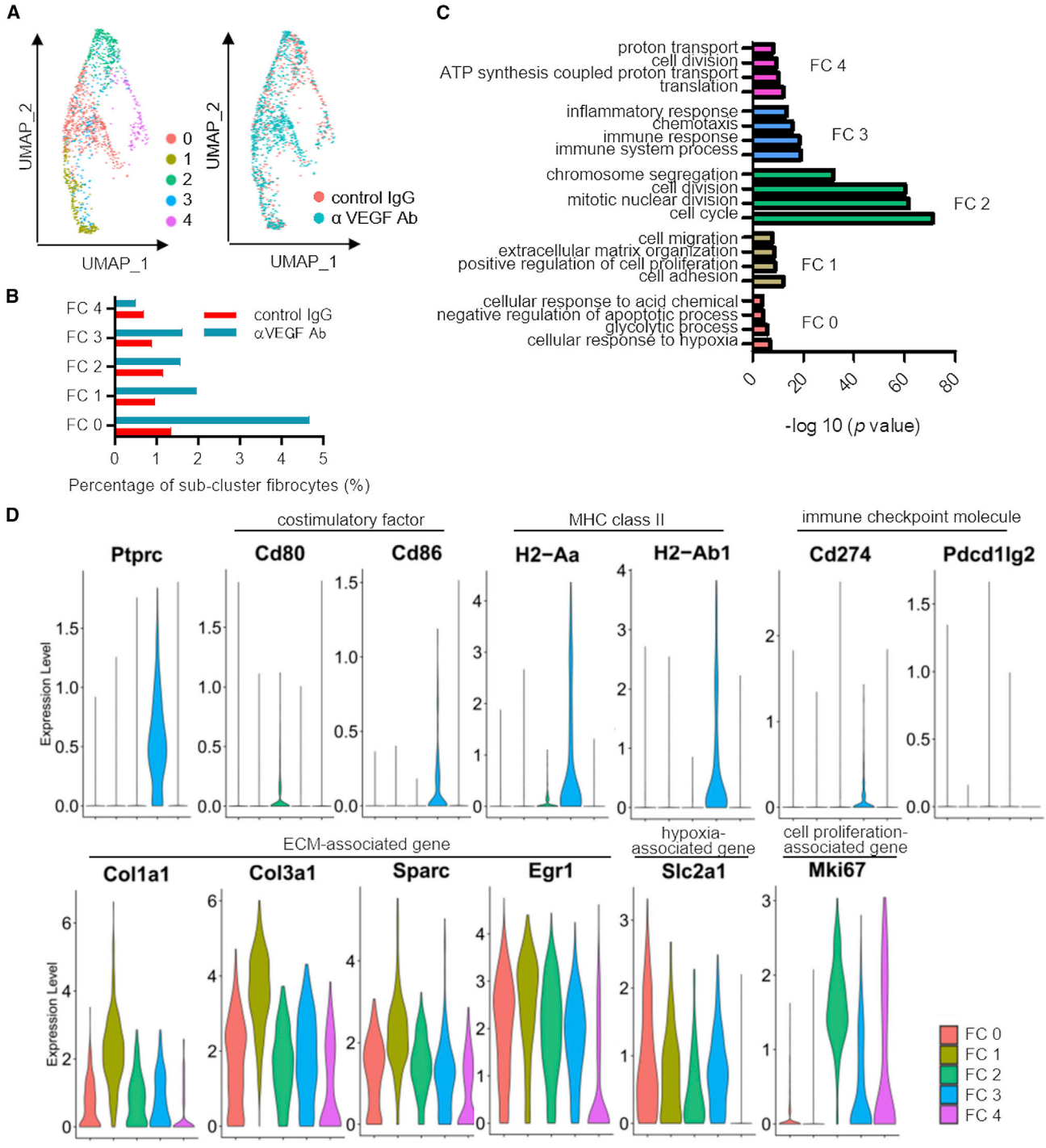

Figure 3. An immune-related subtype of tumor-infiltrating fibrocytes was detected by a single-cell analysis

(A) UMAP plots of fibrocyte clusters showing emergent sub-clusters.

(B) The comparison of each sub-cluster of fibrocytes in isotype control and αVEGF Ab-treated groups.

(C) Gene Ontology identifying pathway enrichment by each sub-group of fibrocytes.

(D) Violin plots of selected genes, showing the normalized expression in each sub-cluster of fibrocytes.

See also Figure S5.

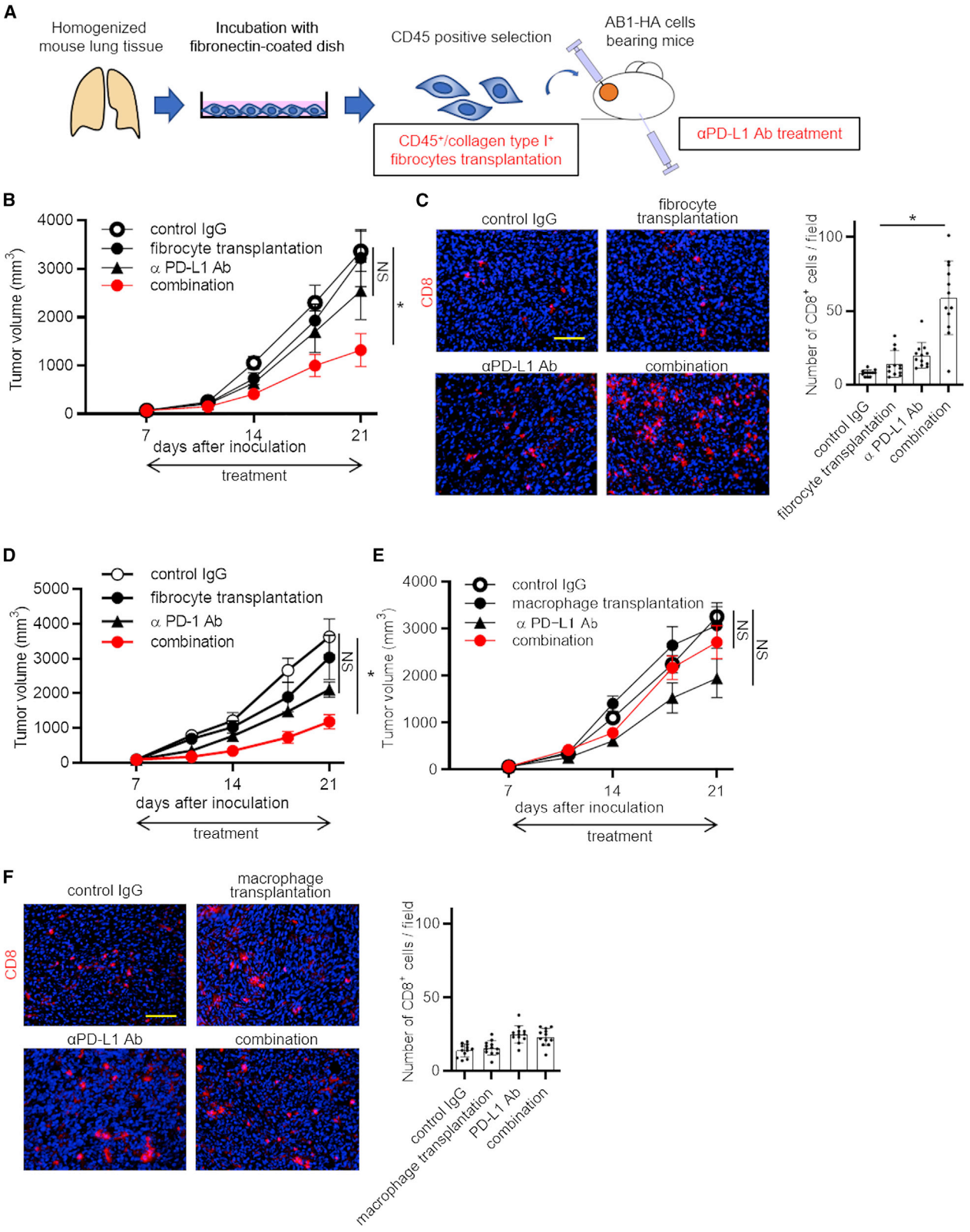

(legend on next page)

(Figure 4D). Furthermore, based on the scRNA-seq results showing increased macrophages in tumor tissue treated with VEGF blockade, we examined the effects of implanting mouse bone marrow-derived macrophages in AB1-HA tumor-bearing mice (Figures 4E and 4F). In contrast with fibrocytes, peritumoral implantation of macrophages tended to inhibit the antitumor effects of PD-L1 blockade (Figure 4E). Macrophage implantation combined with anti-PD-L1 antibody did not increase the tumor-infiltrating $CD8^+$ T cells (Figure 4F). These results suggest that VEGF blockade enhances the antitumor effects of PD-1/PD-L1 blockade, potentially via recruitment of tumor-infiltrating fibrocytes, but not macrophages.

PD-L1 blockade enhanced costimulatory capacity of $CD34^+CD45^+$ fibrocytes in tumor tissue

Analyzing the results of scRNA-seq in AB1-HA tumor tissue revealed the high and specific expression of CD34 in tumor-infiltrating fibrocytes (Figure 5A). This discovery enabled the sorting of tumor-infiltrating fibrocytes as living cells by flow cytometry. For confirmation of the phenotypes of tumor-infiltrating fibrocytes and comparison with macrophages, we isolated $CD34^+CD45^+$ cells as fibrocytes and $CD34^-CD45^+F4/80^+$ cells as macrophages from AB1-HA anti-VEGF antibody-treated tumor tissues (Figure 5B). The frequency of tumor-infiltrating $CD34^+CD45^+$ fibrocytes was increased by VEGF blockade in the flow cytometric analysis (Figure 5C). Considering the results of sub-clustering analysis in tumor-infiltrating fibrocytes (Figure 3D), we identified immune-related FC3 fibrocytes as $CD34^+CD45^+CD86^{high}$ cells. The flow cytometric analysis also revealed that VEGF blockade enhanced the accumulation of FC3 in tumor tissue (Figure 5D). The COL1A1 gene expression of fibrocytes was several-fold higher than that of macrophages, while the CD45 and F4/80 expression was the same (Figure 5E). Furthermore, fibrocytes showed significantly higher expression levels of CD274 (PD-L1) and CD86 in comparison with macrophages. We also isolated $CD34^+CD45^+$ fibrocytes and $CD34^-CD45^+F4/80^+$ macrophages from LLC tumor tissue (Figure S6A). The LLC tumor-derived fibrocytes expressed higher levels of COL1A1 and PD-L1 than macrophages (Figure S6B). We previously reported that lung or peripheral blood fibrocytes had an antigen-presenting ability similar to macrophages and DCs.[18] Thus, tumor-infiltrating fibrocytes and macrophages were isolated by flow cytometry, and their T cell-costimulatory capacities were examined *in vitro*. We performed an allogeneic carboxyfluorescein succinimidyl ester (CFSE) dye dilution mixed lymphocyte reaction assay (CFSE-MLR). $CD8^+$ T cells from C57BL/6 mice were stimulated by tumor-infiltrating fibrocytes from AB1-HA-bearing BALB/c mice treated with anti-VEGF antibody. Tumor-infiltrating fibrocytes augmented the $CD8^+$ T cell proliferation (Figure 5F). Furthermore, PD-L1 blockade significantly enhanced fibrocyte-induced growth of $CD8^+$ T cells (Figure 5G). In contrast, PD-L1 blockade did not upregulate the $CD8^+$ T cell proliferation induced by allogeneic tumor-associated macrophages (TAMs), while TAMs had costimulatory capacity equivalent to or slightly lower than fibrocytes (Figures 5H and 5I).

To investigate whether tumor-infiltrating fibrocytes enhanced T cell proliferation in tumor tissues or draining lymph nodes, we peritumorally transplanted CFSE-labeled lung fibrocytes and tracked their migration. Although bone marrow-derived DCs transplanted in a peritumoral site migrated to draining lymph nodes (subiliac lymph nodes), transplanted fibrocytes were not observed in draining lymph nodes (Figure 5J). We confirmed that both fibrocytes and DCs infiltrated tumor tissue (Figure S7A). Moreover, $Ki67^+$ proliferating T cells were significantly increased in AB1-HA tumor tissues treated with dual VEGF and PD-L1 blockade (Figure 5K). The co-localization of tumor-infiltrating $FSP\text{-}1^+$ fibrocyte-like cells and $CD8^+$ T cells was observed in AB1-HA tumor tissue treated with combined VEGF and PD-L1 blockade (Figure S7B). These results suggested that PD-L1 blockade possibly enhanced the T cell-costimulatory ability of fibrocytes at the local tumor site.

Enhancement of antitumor effects of fibrocytes by PD-L1 blockade was CD86 dependent

We next assessed whether PD-L1 blockade-treated fibrocytes suppressed tumor progression via costimulatory signals in tumor tissue. We previously demonstrated that the antigen-presenting capacity of fibrocytes was partially dependent on CD86 *in vitro*.[18] In the present study, we confirmed that lung-derived fibrocytes expressed cell surface CD86 to the same extent as tumor-infiltrating fibrocytes (Figure S7C). Thus, we peritumorally transferred fibrocytes from the lungs of wild-type (WT) or $CD86^{-/-}$ BALB/c mice into anti-PD-L1 antibody-treated AB1-HA tumor-bearing WT BALB/c mice (Figures 6A and 6B). Although WT fibrocytes augmented the antitumor effects of PD-L1 blockade, synergistic effects were not observed in mice that received implantation of $CD86^{-/-}$ fibrocytes (control IgG versus anti-PD-L1 antibody + WT fibrocyte; $p = 0.008$, control IgG versus anti-PD-L1 antibody + knockout [KO] fibrocyte; $p = 0.309$, day 21 tumor volume). Transplantation of $CD86^{-/-}$ fibrocytes did not affect the number of $CD8^+$ tumor-infiltrating lymphocytes (TILs) in AB1-HA-bearing mice treated with PD-L1

Figure 4. Fibrocyte enhances the antitumor effects of PD-L1 blockade

(A) A diagram showing the strategy of fibrocyte transplantation into tumor site.

(B) The evaluation of the tumor volume of AB1-HA-bearing mice treated with peritumoral fibrocyte transplantation and/or αPD-L1 Ab from 7 days after tumor cell injection (n = 7 per group). *p < 0.05 by one-way ANOVA.

(C) The quantitative evaluation of the number of $CD8^+$ cells per field in each tumor of the mice studied in (B) (n = 15 field per group). Scale bar, 200 μm. *p < 0.05 by one-way ANOVA.

(D) The evaluation of the tumor volume of AB1-HA-bearing mice treated with peritumoral fibrocyte transplantation and/or αPD-1 Ab (200 μg per mouse) from 7 days after tumor cell injection (n = 7 per group). *p < 0.05 by one-way ANOVA.

(E) The evaluation of the tumor volume of AB1-HA-bearing mice treated with peritumoral macrophage transplantation and/or αPD-L1 Ab from 7 days after tumor cell injection (n = 7 per group). *p < 0.05 by one-way ANOVA.

(F) The quantitative evaluation of the number of $CD8^+$ cells per field in each tumor of the mice studied in (E) (n = 12 field per group). Scale bar, 200 μm. *p < 0.05 by one-way ANOVA. The evaluations of immunohistochemical analysis are shown as the mean ± SD. The other data are shown as the mean ± SEM.

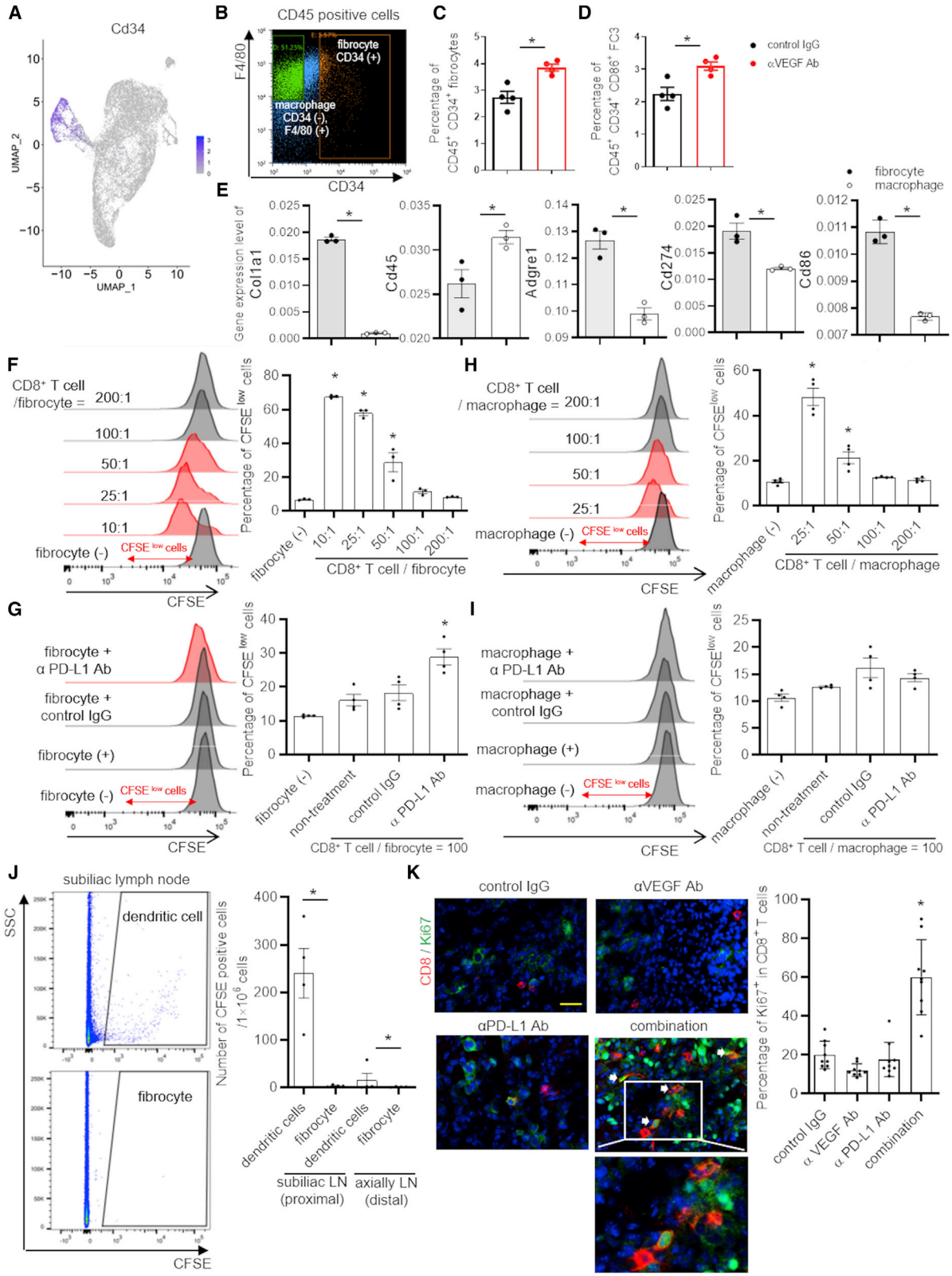

(legend on next page)

blockade (Figure 6C). Both CD80 and CD86 have been known as the main co-stimulatory molecules in APCs. To examine the CD80 dependency in antitumor effects of fibrocytes, we transplanted fibrocytes derived from CD80$^{-/-}$ BALB/c mice (Figure 6D). The implantation of CD80$^{-/-}$ fibrocytes enhanced the antitumor effect of PD-L1 blockade as with WT fibrocytes. Together, these results suggested that the expression of costimulatory molecule CD86, but not CD80, was essential for the antitumor effects and T cell-costimulatory capacity of anti-PD-L1 antibody-treated tumor-infiltrating fibrocytes.

TGF-β/SMAD inhibition enhanced antitumor effects of combination therapy with VEGF and PD-L1 blockade via regulation of fibrocyte differentiation

We next investigated another aspect of tumor-infiltrating fibrocytes as the precursor of fibroblasts. Fibrocytes have been considered to contribute to the pathogenesis of various fibrotic diseases via their differentiation into fibroblasts/myofibroblasts.[12,13,20] However, the process of fibrocyte differentiation in tumor tissue is unclear. We therefore analyzed the developmental trajectory of tumor-infiltrating CD45$^+$ cells (10,142 cells sequenced) in AB1-HA-bearing mice treated with anti-PD-L1 and anti-VEGF antibodies (Figures 7A–7C). A pseudotime analysis of scRNA-seq data revealed that the features of monocytes/macrophages (CXCR4, MRC-1) decreased along the trajectories, while fibrocyte/fibroblast markers (collagens, CD34) increased. These results indicated that tumor-infiltrating myeloid cells, including fibrocytes, had the capacity to acquire fibroblastic phenotypes in tumor tissue, whereas they lost immune cell phenotypes. Considering that CAF had a huge impact on tumor progression,[21,22] we hypothesized that the inhibition of fibrocyte differentiation into fibroblasts enhanced the antitumor effects of combined blockade of PD-L1 and VEGF. To preserve the immune cell phenotypes of fibrocytes, we next explored the key regulator in the differentiation of tumor-infiltrating fibrocytes. We predicted the transcription regulators of tumor-infiltrating fibrocytes and macrophages by the weighted parametric gene set analysis (wPGSA) method.[23] Analyzing the differentially expressed genes in each cluster, the results of wPGSA predicted that small mothers against decapentaplegic (SMAD) 1/4 activity in tumor-infiltrating fibrocytes was increased in comparison with M1-like and M2-like TAMs (Figure 7D). The transforming growth factor β (TGF-β)/SMAD pathway is reportedly a key regulator of fibroblast activation and differentiation into myofibroblasts.[21,24] Furthermore, recent studies suggested that TGF-β induced human circulating fibrocytes to acquire myofibroblast-like phenotypes (e.g., high ECM production and alpha-smooth muscle actin [αSMA] expression).[12,20] To confirm whether tumor-infiltrating fibrocytes had the capacity to differentiate into the myofibroblast-like lineage via the TGF-β/SMAD signaling pathway, we isolated CD45$^+$CD34$^+$ tumor-infiltrating fibrocytes from AB1-HA-bearing mice and treated them with 10 ng/mL TGF-β for 7 days (Figures 7E and 7F). TGF-β induced the morphological change of spindle-shaped fibrocytes to well-spread/polygonal-shaped cells known as myofibroblasts (Figure 7E),[21,24] whereas the morphology of TAMs was unchanged. Furthermore, the gene expression levels of COL1A1 and αSMA were increased by TGF-β (Figure 7F). The present results revealed the capability of tumor-infiltrating fibrocytes to differentiate into myofibroblast-like cells in response to TGF-β, which was distinct from macrophages. Therefore, we next examined the antitumor effect of combination therapy with anti-VEGF antibody, anti-PD-L1 antibody, and TGF-β/SMAD inhibitor *in vivo* (Figure 7G). We orally administered a TGF-βR/SMAD inhibitor (SB525334) once daily (6 days on/1 day off) to AB1-HA-bearing mice. TGF-βR/SMAD inhibitor monotherapy did not suppress tumor progression *in vivo* (Figure 7G). However, TGF-βR/SMAD inhibitor significantly enhanced the antitumor effect of anti-VEGF antibody and anti-PD-L1 antibody combination therapy. Furthermore, anti-VEGF antibody/anti-PD-L1 antibody/SB525334 combination therapy increased the tumor-infiltrating CD8$^+$ T cells in AB1-HA tumors (Figure 7H). Based on the hypothesis that TGF-βR/SMAD inhibitor suppresses the differentiation of fibrocytes into myofibroblasts, we evaluated tumor-infiltrating fibrocytes (Figure 7I) and αSMA$^+$ myofibroblasts (Figure 7J). The addition of TGF-βR/SMAD inhibitor increased the accumulation of collagen1a1$^+$CD45$^+$ fibrocytes that occurred with VEGF blockade, whereas αSMA$^+$ myofibroblasts were decreased. Taken together, the present results indicated that TGF-β/SMAD signaling pathway inhibition augmented the antitumor effects

Figure 5. PD-L1 blockade augments the CD8$^+$ T cell costimulation of CD34$^+$CD45$^+$ fibrocytes at the tumor site

(A) UMAP plots of CD34 in scRNA-seq data generated from CD45$^+$ cells in AB1-HA tumor tissue.

(B) The isolation of fibrocytes (CD34$^+$CD45$^+$ cells) and macrophages (CD34$^-$CD45$^+$F4/80$^+$ cells) from AB1-HA tumor tissue treated with αVEGF Ab.

(C and D) Flow cytometry of CD34$^+$ CD45$^+$ fibrocytes (C) and CD34$^+$CD45$^+$CD86$^+$ FC3 (D) in tumor tissue derived from AB1-HA tumor-bearing mice treated with control IgG or VEGF blockade (5 mg/kg).

(E) The gene expression levels of fibrocyte markers, PD-L1, and CD86 in tumor-infiltrating fibrocytes and macrophages (n = 3 per group). *p < 0.05 by Student's t test.

(F) The mouse allogeneic mixed lymphocyte reaction assay (MLR) of CD8$^+$ T cells co-cultured with tumor-infiltrating fibrocytes (n = 4 per group).

(G) The effects of anti-PD-L1 antibody in mouse allogeneic MLR stimulated with tumor-infiltrating fibrocytes (n = 4 per group). *p < 0.05 by one-way ANOVA.

(H) The mouse allogeneic MLR of CD8$^+$ T cells co-cultured with tumor-associated macrophages isolated in (B). The proliferation of CFSE-labeled CD8$^+$ T cells was determined based on CFSE dilution after 4 days of co-culture (n = 4 per group). *p < 0.05 by one-way ANOVA.

(I) The effects of anti-PD-L1 antibody in mouse allogeneic MLR stimulated with tumor-associated macrophages (n = 4 per group). *p < 0.05 by one-way ANOVA.

(J) The tracking of lung fibrocytes and bone marrow dendritic cells to tumor draining lymph nodes *in vivo* (n = 5 per group). CFSE-labeled antigen-presenting cells were peritumorally transplanted in AB1-HA tumor-bearing mice, and the number of cells that migrated to the lymph nodes was evaluated 48 h later. *p < 0.05 by the Mann-Whitney *U* test.

(K) Double staining of CD8a and Ki67 in tumors from mice treated with low-dose αVEGF Ab and/or αPD-L1 Ab (studied in Figure 1C). Scale bar, 50 μm. White arrows indicate the proliferating CD8$^+$ T cells. The number of double-positive cells in tumors was evaluated in each group. *p < 0.05 by one-way ANOVA. The evaluations of immunohistochemical analysis are shown as the mean ± SD. The other data are shown as the mean ± SEM.

See also Figures S6 and S7.

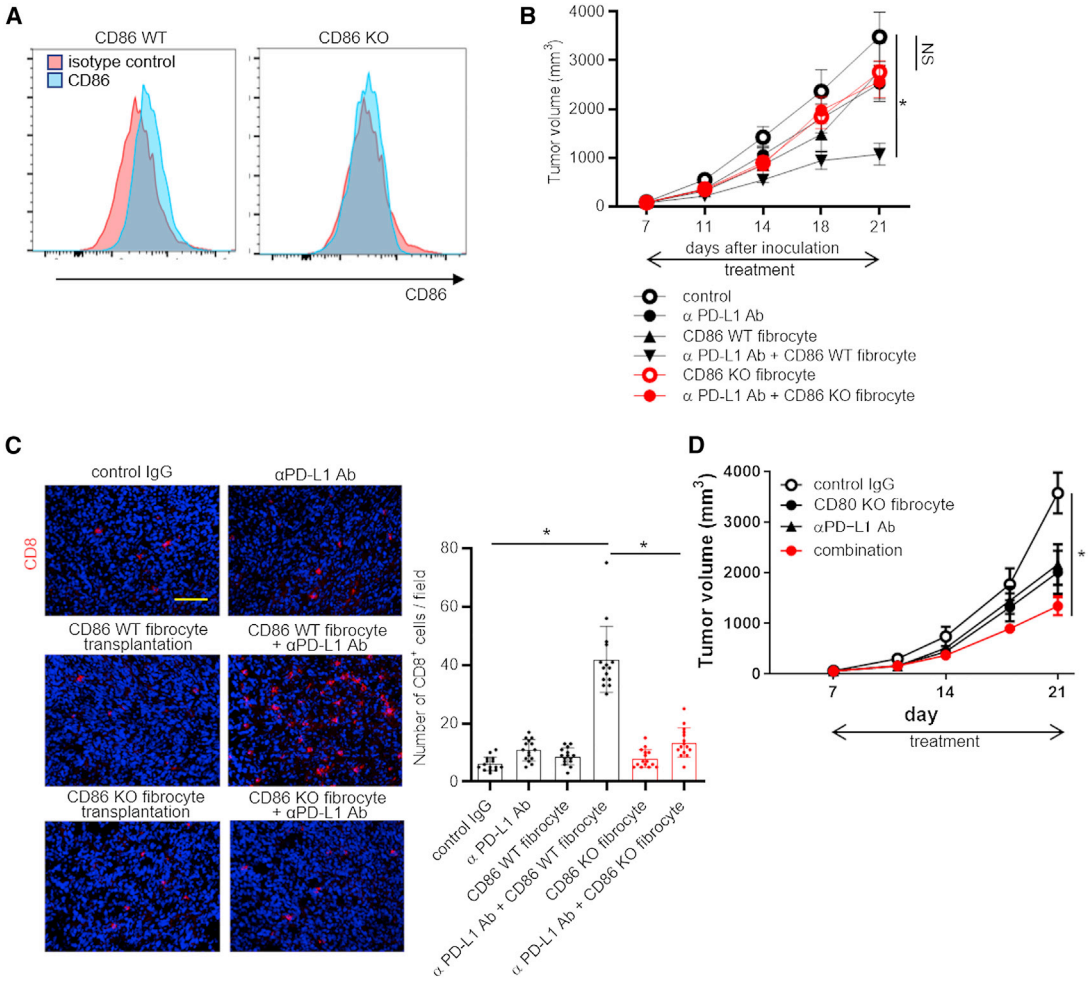

Figure 6. CD86 deficiency attenuates the antitumor function of fibrocytes in PD-L1 immunotherapy

(A) A representative flow cytometric analysis of the CD86 expression on lung fibrocytes from CD86-WT or CD86-KO mice.

(B) The evaluation of the tumor volume of AB1-HA-bearing mice treated with peritumoral transplantation of fibrocytes from CD86-WT or CD86-KO mice and/or an αPD-L1 Ab from 7 days after tumor cell injection (n = 7 per group). *p < 0.05 by one-way ANOVA.

(C) The quantitative evaluation of the number of $CD8^+$ cells per field in each tumor of mice studied in (B) (n = 15 field per group). Scale bar, 200 μm. *p < 0.05 by one-way ANOVA.

(D) The evaluation of the tumor volume of AB1-HA-bearing mice treated with peritumoral transplantation of fibrocytes from CD80-KO mice and/or an αPD-L1 Ab from 7 days after tumor cell injection (n = 7 per group). *p < 0.05 by one-way ANOVA. The evaluations of immunohistochemical analysis are shown as the mean ± SD. The other data are shown as the mean ± SEM.

of anti-VEGF antibody and anti-PD-L1 antibody combination treatment by regulating fibrocyte differentiation.

DISCUSSION

For more than a decade, fibrocytes have attracted attention for their roles as an ECM producer and fibroblast precursor in wound healing and fibrotic diseases. In contrast, little is known about their role in tumor sites and their other function as immune cells. Furthermore, the scientific landscape of blurred outlines regarding fibrocytes was due to difficulties in directly harvesting fibrocytes from tissues as living cells and depleting them with specific markers in mouse models. Instead, we used intracellular collagen staining of fixed fibrocytes, or culturing in a fibronectin-coated dish with peripheral blood mononuclear cells. We herein identified "fibrocyte clusters" in tumor tissues by scRNA-seq, purified living fibrocytes, and analyzed the immunological function and roles in tumor immunity, particularly in combination therapy with ICIs and VEGF blockade.

Using scRNA-seq, we herein demonstrated, for the first time, the "fibrocyte cluster," which is fairly independent from other clusters (including macrophages) in tumor tissues. The results strongly indicate the existence of large numbers of fibrocytes in tumors and a unique cell population that differs from other hematopoietic lineage cells. The data may have the potential to end the debate on their difference from macrophages. Furthermore,

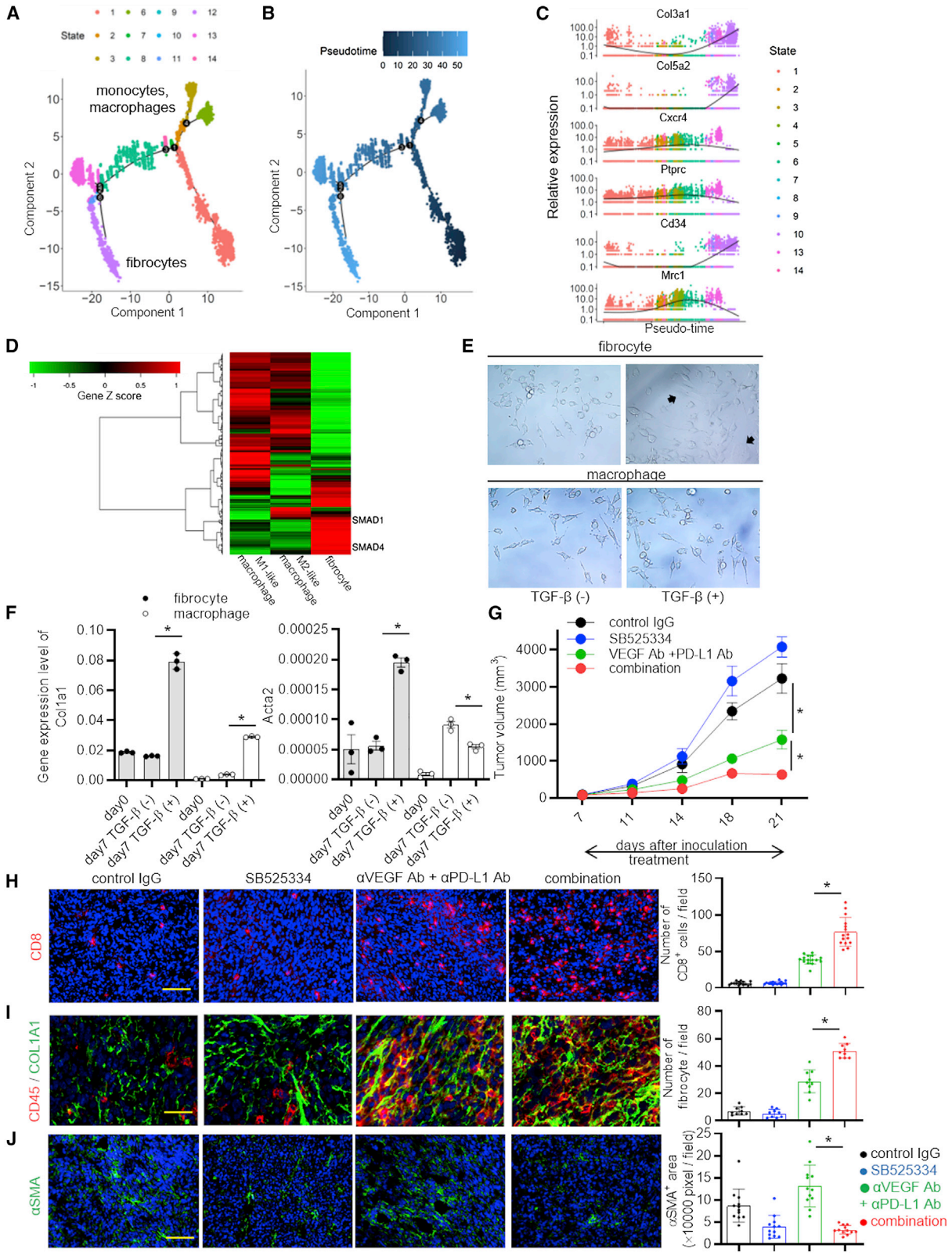

(legend on next page)

directly purified fibrocytes from tumors, as $CD45^+CD34^+$ cells, showed a similar phenotype to fibrocytes that we and others generated *in vitro*.[18,25]

Chesney et al.[17] reported that the antigen-presenting capacity of peripheral blood fibrocytes is close to that of DCs. Recently, we showed that fibrocytes harvested by a culturing method had antigen-presenting abilities and its augmentation by PD-1/PD-L1 blockade.[18] Consistent with our previous data,[18] the present data indicated that directly harvested tumor-infiltrating fibrocytes had T cell-costimulatory activities that were higher than those of TAMs.

Several reports have shown that the PD-L1 expression in tumor-associated APCs, including macrophages and DCs, governs the antitumor effects of PD-1/PD-L1 blockade. Liu et al.[26] showed that the colocalization of PD-L1 and TAM in NSCLC tumor tissue was correlated with better clinical outcomes of ICI. Gordon et al.[27] revealed that the PD-1 expression in TAMs restricted their phagocytosis, and PD-1/PD-L1 blockade enhanced the antitumor ability of TAMs. More recently, Petty et al.[28] demonstrated that the expression of PD-L1 on TAMs suppressed the functions of $CD8^+$ TILs in *PDL1* conditional KO mice crossed with *LysM-cre* and $PDL1^{fl/fl}$ mice. However, this was discordant with our data showing that PD-L1 blockade did not enhance the T cell-costimulatory ability or antitumor effect of tumor-derived $F4/80^+CD34^-$ macrophages *in vitro* or *in vivo*. In addition to the report showing that the expression of lysozyme M was not limited in macrophages,[29] our scRNA-seq data showed that the expression of *Lyz2* gene in fibrocyte clusters, particularly in sub-cluster FC3 (immune-related fibrocytes), was comparable with that of macrophages (Figures 2D and S5). Because tumor-infiltrating fibrocytes also expressed macrophage markers (e.g., CD68 and F4/80), the cells widely known as TAMs could contain fibrocytes. Therefore, the present study proposed the importance of discriminating fibrocytes from macrophages by CD34 expression to investigate the correct phenotypes of each population. Further experiments are required to explore the details of tumor-infiltrating fibrocytes.

On the other hand, previous reports have indicated that TAMs have relatively weak effects on T cell priming in the tumor microenvironment, but that the PD-L1 expression in DCs regulated the antitumor $CD8^+$ T cell response.[30–32] Our study demonstrated that DCs transplanted into tumor sites showed the capacity to migrate to draining lymph nodes, whereas fibrocytes did not. These data suggest the different roles of DCs and fibrocytes as APCs. DCs play a role in the priming of naive T cells in draining lymph nodes, whereas fibrocytes may serve to re-stimulate effector T cells in tumor sites. This hypothesis was supported by scRNA-seq data indicating that, in tumor sites, DC clusters were very small and the number of fibrocytes (1,491 cells) was much higher than the number of DCs (115 cells). We also showed that the antigen-presenting capacity of fibrocytes was CD86 dependent because $CD86^{-/-}$ fibrocytes failed to show antitumor effects in combination with anti-PD-L1 antibody. The expression pattern with $CD80^{low}$ and $CD86^{high}$ seems to be characteristic of APCs working in tumor sites, like fibrocytes, which differs from $CD80^{high}$ DCs, to prevent PD-L1 signaling via *cis*-PD-L1/CD80 interactions on APCs.[33,34]

A recent study identified sub-populations of cancer-associated fibroblasts (CAFs) that enhance antitumor immunity. Öhlund et al.[35] revealed the presence of αSMA^{high} myofibroblastic CAFs (myCAFs) and $\alpha SMA^{low}IL\text{-}6^{high}$ inflammatory CAFs (iCAFs) in pancreatic ductal adenocarcinoma. Furthermore, Elyada et al.[36] reported that antigen-presenting CAFs (apCAFs) activated $CD4^+$ T cells via antigen presentation in tumor tissues. It is unclear whether apCAFs may be in the differentiation lineage of tumor-infiltrating fibrocytes, particularly sub-cluster FC3 (immune-related fibrocytes). Of course, tumor-infiltrating fibrocytes expressed common CAF markers, including collagens, vimentin, and podoplanin (Figure S5). In contrast, the majority did not express markers of iCAF, myCAF, or apCAF. FC3 partially expressed iCAF (Col14a1) and apCAF (Cd74) markers. However, FC3 also expressed the macrophage markers (e.g., F4/80 and CD68) in addition to CD45, which are not expressed in fibroblasts. A lineage tracing study and large-scale scRNA-seq with all cells in tumor tissues will clarify this.

VEGF/VEGFR blockade has been reported to modify the tumor microenvironment by inhibiting the recruitment and/or function of tumor-infiltrating inhibitory immune cells, such as M2-macrophages, T_{reg}s, and MDSCs.[4–8] In this study, VEGF blockade increased the accumulation of M1-like macrophages and fibrocytes, but reduced MDSCs in tumors. Because tumor-infiltrating fibrocytes showed higher levels of T cell-costimulatory activity

Figure 7. TGF-β/SMAD inhibitor enhanced the antitumor effects of dual VEGF and PD-L1 blockade via regulation of fibrocyte differentiation

(A and B) Monocle-generated plots presenting differentiation trajectory (A) and pseudotime ordering (B) of tumor-infiltrating $CD45^+$ cells from AB1-HA tumor tissue treated with dual blockade of VEGF (1 mg/kg) and PD-L1 (5 mg/kg).

(C) Monocle-generated plots showing the pseudotime-ordered expression of selected marker genes. Lines show the relative expression of each marker in pseudotime.

(D) A cluster map of relative transcription factor activities in tumor-infiltrating fibrocytes and macrophages clusters was estimated using wPGSA from the samples studied in Figure 2.

(E) Representative images of tumor-infiltrating fibrocytes ($CD34^+CD45^+$ cells) and macrophages ($CD34^-CD45^+F4/80^+$ cells) from AB1-HA tumor tissue treated with αVEGF Ab.

(F) The gene expression levels of COL1A1 and ACTA2 in the tumor-infiltrating fibrocytes and macrophages (n = 3 per group). *$p < 0.05$ by Student's t test.

(G) The evaluation of the tumor volume of AB1-HA-bearing mice treated with low-dose αVEGF Ab and αPD-L1 Ab and/or SB525334 (n = 7 per group). *$p < 0.05$ by one-way ANOVA.

(H) Representative images and quantitative evaluation of sections from AB1-HA tumors stained for CD8a. The tumors were harvested from each group in (D) on day 21. Scale bar, 200 μm. *$p < 0.05$ by one-way ANOVA.

(I) Double staining of collagen1a1 and CD45 in AB1-HA tumors on day 21. Scale bar, 50 μm. The number of double-positive cells in the tumors was evaluated (n = 9 field per group).

(J) Representative images and quantitative evaluation of sections from AB1-HA tumors stained for αSMA (n = 12 field per group). Scale bar, 200 μm. *$p < 0.05$ by one-way ANOVA. The evaluations of immunohistochemical analysis are shown as the mean ± SD. The other data are shown as the mean ± SEM.

than macrophages, particularly in combination with anti-PD-L1 antibody, and the number in tumor tissues was higher than those DCs, they may centrally contribute *in situ* to the synergistic antitumor effects of VEGF/VEGFR and PD-1/PD-L1 blockade, in addition to MDSCs, T_{reg}s, and TAMs.

To further develop more effective tumor immunotherapy, our data remind us to increase immune-related fibrocytes in tumors when PD-1/PD-L1 blockade is applied. For this purpose, we searched for transcription regulators of tumor-infiltrating fibrocytes, which are activated in tumor sites, and identified SMAD1/4 activity. Several recent studies revealed that TGF-β/SMAD signaling negatively affected antitumor immunity. Tumor-derived TGF-β is known to suppress the expression of cytolytic gene products and upregulate PD-1 in T cells.[37–39] Furthermore, Grauel et al.[40] demonstrated that TGF-β blockade regulated the plasticity of CAFs and augmented the efficacy of anti-PD-1 antibody. Because dual-target inhibition of the PD-1/PD-L1 and TGF-β/SMAD axis has been considered as a promising antitumor strategy, several clinical trials are ongoing.[41–43] This study prompted a reevaluation of TGF-β/SMAD inhibitor, which enhanced the antitumor effects of dual VEGF and PD-L1 blockade through the regulation of fibrocyte differentiation. Furthermore, our pseudotime analysis indicated that fibrocytes lost their immune cell-like features as they differentiated into myofibroblast-like populations. Taken together, triple-combination therapy with anti-VEGF antibody, anti-PD-L1 antibody, and TGF-β/SMAD inhibitor could optimize the antitumor effects of fibrocytes via recruitment, supporting T cell priming, and maintaining the features as immune cells, respectively.

The present study has potential clinical implications. First, our clinical and preclinical data identified fibrocytes as a novel APC in the tumor microenvironment. Moreover, tumor-infiltrating fibrocytes had distinct properties from known APCs (e.g., DCs and TAMs). A novel concept, the control of tumor-infiltrating fibrocytes, could accelerate the development of immunotherapy. Second, we revealed that VEGF blockade and TGF-β/SMAD inhibitor regulated the accumulation and differentiation of fibrocytes, respectively. Thus, triple-combination therapy with anti-PD-L1 antibody, anti-VEGF antibody, and TGF-β/SMAD inhibitor could be a promising cancer treatment strategy. Third, fibrocytes, particularly FC3, may be a biomarker for the therapeutic effect of PD-1/PD-L1 antibodies, although fibrocytes originally have the potential to promote tumor progression.[15]

In conclusion, we identified fibrocytes as a novel tumor-associated APC that governed the therapeutic effect of anti-PD-1/PD-L1 antibodies. Our findings highlighted the control of tumor-infiltrating fibrocytes as an important approach for the advancement of combination immunotherapy.

Limitations of the study

In this study, we demonstrate that tumor-infiltrating fibrocytes are an attractive immunotherapeutic target to determine the efficacy of combination immunotherapy. Some limitations of the study include the detail characteristics of tumor-infiltrating fibrocytes compared with circulating fibrocytes. In particular, the roles of sub-clusters in tumor-infiltrating fibrocytes were not fully elucidated. The specific markers and the differentiation mechanisms of each sub-cluster should be addressed in a future study. In addition, the studies of fibrocyte transplantation were performed with lung-derived fibrocytes because of the limitation of the available number of tumor-derived fibrocytes.

STAR★METHODS

Detailed methods are provided in the online version of this paper and include the following:

- KEY RESOURCES TABLE
- RESOURCE AVAILABILITY
  - Lead contact
  - Materials availability
  - Data and code availability
- EXPERIMENTAL MODEL AND SUBJECT DETAILS
  - Cell lines
  - Animals
  - Clinical sample
- METHOD DETAILS
  - Reagents
  - Animal experiments
  - Purification of mouse lung fibrocytes
  - Purification of mouse macrophages
  - Purification of tumor-infiltrating immune cells
  - Purification of bone marrow-derived dendritic cells
  - *In vivo* tracking of fibrocytes and dendritic cells
  - qRT-PCR
  - Single-cell RNA sequencing
  - Immunohistochemical studies
  - Immunofluorescence staining
  - Flow cytometry
  - Proliferation assay of $CD8^+$ T cells
- QUANTIFICATION AND STATISTICAL ANALYSIS

SUPPLEMENTAL INFORMATION

Supplemental information can be found online at https://doi.org/10.1016/j.celrep.2023.112162.

ACKNOWLEDGMENTS

We thank our colleagues at The University of Tokushima, especially A. Tanabe and R. Akutagawa for their technical assistance and the members of the Nishioka Lab for their technical advice and fruitful discussions. We also thank S. Tsukumo at Department of Immunology and Parasitology, Graduate School of Medicine, Tokushima University for the technical advice on scRNA-seq. This study was supported by the Support Center for Advanced Medical Sciences, Tokushima University Graduate School of Biomedical Sciences. This study was supported by Japan Society for the Promotion of Science (JSPS) KAKENHI Grant 16H05309, 19H03668, 22H03079, a Grant-in-Aid for Scientific Research (B) from the JSPS, Japan (to Y.N.), SPS KAKENHI Grant 19K16746, a Grant-in-Aid for Early-Career Scientists from Japan Society for the Promotion of Science (JSPS), Japan (to A.M.), and a grant to the Diffuse Lung Diseases Research Group from the Ministry of Health, Labour and Welfare, Japan (to Y.N.). This study was supported by Chugai Pharmaceutical, Co., Ltd.

AUTHOR CONTRIBUTIONS

A.M. and Y.N. designed, planned, and coordinated the experiments and wrote the manuscript. A.M. performed and analyzed the experiments with K.K., H.O.,

T.A., N.T.N., and H.Y.; K.O., M.S., O.K., H.N., T.S., M.H., H.T., and Y.N. supervised the project. All authors edited or commented on the manuscript.

DECLARATION OF INTERESTS

Y.N. reports research fees paid to his institution and personal fees from Chugai Pharmaceutical Co., Ltd. M.S. and O.K. are employees of Chugai Pharmaceutical Co., Ltd. The other authors declare no conflicts of interest in association with the present study.

Received: February 17, 2022
Revised: December 28, 2022
Accepted: February 9, 2023
Published: March 3, 2023

REFERENCES

1. Rittmeyer, A., Barlesi, F., Waterkamp, D., Park, K., Ciardiello, F., von Pawel, J., Gadgeel, S.M., Hida, T., Kowalski, D.M., Dols, M.C., et al. (2017). Atezolizumab versus docetaxel in patients with previously treated non-small-cell lung cancer (OAK): a phase 3, open-label, multicentre randomised controlled trial. Lancet *389*, 255–265. https://doi.org/10.1016/S0140-6736(16)32517-X.
2. Havel, J.J., Chowell, D., and Chan, T.A. (2019). The evolving landscape of biomarkers for checkpoint inhibitor immunotherapy. Nat. Rev. Cancer *19*, 133–150. https://doi.org/10.1038/s41568-019-0116-x.
3. Meric-Bernstam, F., Larkin, J., Tabernero, J., and Bonini, C. (2021). Enhancing anti-tumour efficacy with immunotherapy combinations. Lancet *397*, 1010–1022. https://doi.org/10.1016/S0140-6736(20)32598-8.
4. Georganaki, M., van Hooren, L., and Dimberg, A. (2018). Vascular targeting to increase the efficiency of immune checkpoint blockade in cancer. Front. Immunol. *9*, 3081. https://doi.org/10.3389/fimmu.2018.03081.
5. Lee, W.S., Yang, H., Chon, H.J., and Kim, C. (2020). Combination of anti-angiogenic therapy and immune checkpoint blockade normalizes vascular-immune crosstalk to potentiate cancer immunity. Exp. Mol. Med. *52*, 1475–1485. https://doi.org/10.1038/s12276-020-00500-y.
6. Popat, S., Grohé, C., Corral, J., Reck, M., Novello, S., Gottfried, M., Radonjic, D., and Kaiser, R. (2020). Anti-angiogenic agents in the age of resistance to immune checkpoint inhibitors: do they have a role in non-oncogene-addicted non-small cell lung cancer? Lung Cancer *144*, 76–84. https://doi.org/10.1016/j.lungcan.2020.04.009.
7. Socinski, M.A., Jotte, R.M., Cappuzzo, F., Orlandi, F., Stroyakovskiy, D., Nogami, N., Rodríguez-Abreu, D., Moro-Sibilot, D., Thomas, C.A., Barlesi, F., et al. (2018). Atezolizumab for first-line treatment of metastatic nonsquamous NSCLC. N. Engl. J. Med. *378*, 2288–2301. https://doi.org/10.1056/NEJMoa1716948.
8. Rini, B.I., Powles, T., Atkins, M.B., Escudier, B., McDermott, D.F., Suarez, C., Bracarda, S., Stadler, W.M., Donskov, F., Lee, J.L., et al. (2019). Atezolizumab plus bevacizumab versus sunitinib in patients with previously untreated metastatic renal cell carcinoma (IMmotion151): a multicentre, open-label, phase 3, randomised controlled trial. Lancet *393*, 2404–2415. https://doi.org/10.1016/S0140-6736(19)30723-8.
9. Finn, R.S., Qin, S., Ikeda, M., Galle, P.R., Ducreux, M., Kim, T.Y., Kudo, M., Breder, V., Merle, P., Kaseb, A.O., et al. (2020). Atezolizumab plus bevacizumab in unresectable hepatocellular carcinoma. N. Engl. J. Med. *382*, 1894–1905. https://doi.org/10.1056/NEJMoa1915745.
10. Rahma, O.E., and Hodi, F.S. (2019). The intersection between tumor angiogenesis and immune suppression. Clin. Cancer Res. *25*, 5449–5457. https://doi.org/10.1158/1078-0432.CCR-18-1543.
11. de Almeida, P.E., Mak, J., Hernandez, G., Jesudason, R., Herault, A., Javinal, V., Borneo, J., Kim, J.M., and Walsh, K.B. (2020). Anti-VEGF treatment enhances $CD8^+$ T-cell antitumor activity by amplifying hypoxia. Cancer Immunol. Res. *8*, 806–818. https://doi.org/10.1158/2326-6066.CIR-19-0360.
12. Reilkoff, R.A., Bucala, R., and Herzog, E.L. (2011). Fibrocytes: emerging effector cells in chronic inflammation. Nat. Rev. Immunol. *11*, 427–435. https://doi.org/10.1038/nri2990.
13. Schmidt, M., Sun, G., Stacey, M.A., Mori, L., and Mattoli, S. (2003). Identification of circulating fibrocytes as precursors of bronchial myofibroblasts in asthma. J. Immunol. *171*, 380–389. https://doi.org/10.4049/jimmunol.171.1.380.
14. Odackal, J., Yu, V., Gomez-Manjerres, D., Field, J.J., Burdick, M.D., and Mehrad, B. (2020). Circulating fibrocytes as prognostic biomarkers of autoimmune interstitial lung disease. ERJ Open Res. *6*, 00481–02020. https://doi.org/10.1183/23120541.00481-2020.
15. Saijo, A., Goto, H., Nakano, M., Mitsuhashi, A., Aono, Y., Hanibuchi, M., Ogawa, H., Uehara, H., Kondo, K., and Nishioka, Y. (2018). Bone marrow-derived fibrocytes promote stem cell-like properties of lung cancer cells. Cancer Lett. *421*, 17–27. https://doi.org/10.1016/j.canlet.2018.02.016.
16. Mitsuhashi, A., Goto, H., Saijo, A., Trung, V.T., Aono, Y., Ogino, H., Kuramoto, T., Tabata, S., Uehara, H., Izumi, K., et al. (2015). Fibrocyte-like cells mediate acquired resistance to anti-angiogenic therapy with bevacizumab. Nat. Commun. *6*, 8792. https://doi.org/10.1038/ncomms9792.
17. Chesney, J., Bacher, M., Bender, A., and Bucala, R. (1997). The peripheral blood fibrocyte is a potent antigen-presenting cell capable of priming naive T cells in situ. Proc. Natl. Acad. Sci. USA *94*, 6307–6312. https://doi.org/10.1073/pnas.94.12.6307.
18. Afroj, T., Mitsuhashi, A., Ogino, H., Saijo, A., Otsuka, K., Yoneda, H., Tobiume, M., Nguyen, N.T., Goto, H., Koyama, K., et al. (2021). Blockade of PD-1/PD-L1 pathway enhances the antigen-presenting capacity of fibrocytes. J. Immunol. *206*, 1204–1214. https://doi.org/10.4049/jimmunol.2000909.
19. Abe, R., Donnelly, S.C., Peng, T., Bucala, R., and Metz, C.N. (2001). Peripheral blood fibrocytes: differentiation pathway and migration to wound sites. J. Immunol. *166*, 7556–7562. https://doi.org/10.4049/jimmunol.166.12.7556.
20. Hong, K.M., Belperio, J.A., Keane, M.P., Burdick, M.D., and Strieter, R.M. (2007). Differentiation of human circulating fibrocytes as mediated by transforming growth factor-beta and peroxisome proliferator-activated receptor gamma. J. Biol. Chem. *282*, 22910–22920. https://doi.org/10.1074/jbc.M703597200.
21. Sahai, E., Astsaturov, I., Cukierman, E., DeNardo, D.G., Egeblad, M., Evans, R.M., Fearon, D., Greten, F.R., Hingorani, S.R., Hunter, T., et al. (2020). A framework for advancing our understanding of cancer-associated fibroblasts. Nat. Rev. Cancer *20*, 174–186. https://doi.org/10.1038/s41568-019-0238-1.
22. Lakins, M.A., Ghorani, E., Munir, H., Martins, C.P., and Shields, J.D. (2018). Cancer-associated fibroblasts induce antigen-specific deletion of CD8+ T Cells to protect tumour cells. Nat. Commun. *9*, 948. https://doi.org/10.1038/s41467-018-03347-0.
23. Kawakami, E., Nakaoka, S., Ohta, T., and Kitano, H. (2016). Weighted enrichment method for prediction of transcription regulators from transcriptome and global chromatin immunoprecipitation data. Nucleic Acids Res. *44*, 5010–5021. https://doi.org/10.1093/nar/gkw355.
24. Khouw, I.M., van Wachem, P.B., Plantinga, J.A., Vujaskovic, Z., Wissink, M.J., de Leij, L.F., and van Luyn, M.J. (1999). TGF-beta and bFGF affect the differentiation of proliferating porcine fibroblasts into myofibroblasts in vitro. Biomaterials *20*, 1815–1822. https://doi.org/10.1016/s0142-9612(99)00077-0.
25. Pilling, D., Fan, T., Huang, D., Kaul, B., and Gomer, R.H. (2009). Identification of markers that distinguish monocyte-derived fibrocytes from monocytes, macrophages, and fibroblasts. PLoS One *4*, e7475. https://doi.org/10.1371/journal.pone.0007475.
26. Liu, Y., Zugazagoitia, J., Ahmed, F.S., Henick, B.S., Gettinger, S.N., Herbst, R.S., Schalper, K.A., and Rimm, D.L. (2020). Immune cell PD-L1 colocalizes with macrophages and is associated with outcome in PD-1

pathway blockade therapy. Clin. Cancer Res. *26*, 970–977. https://doi.org/10.1158/1078-0432.CCR-19-1040.

27. Gordon, S.R., Maute, R.L., Dulken, B.W., Hutter, G., George, B.M., McCracken, M.N., Gupta, R., Tsai, J.M., Sinha, R., Corey, D., et al. (2017). PD-1 expression by tumour-associated macrophages inhibits phagocytosis and tumour immunity. Nature *545*, 495–499. https://doi.org/10.1038/nature22396.
28. Petty, A.J., Dai, R., Lapalombella, R., Baiocchi, R.A., Benson, D.M., Li, Z., Huang, X., and Yang, Y. (2021). Hedgehog-induced PD-L1 on tumor-associated macrophages is critical for suppression of tumor-infiltrating $CD8^+$ T cell function. JCI Insight *6*, e146707. https://doi.org/10.1172/jci.insight.146707.
29. Cuda, C.M., Agrawal, H., Misharin, A.V., Haines, G.K., 3rd., Hutcheson, J., Weber, E., Schoenfeldt, J.A., Mohan, C., Pope, R.M., and Perlman, H. (2012). Requirement of myeloid cell-specific Fas expression for prevention of systemic autoimmunity in mice. Arthritis Rheum. *64*, 808–820. https://doi.org/10.1002/art.34317.
30. Peng, Q., Qiu, X., Zhang, Z., Zhang, S., Zhang, Y., Liang, Y., Guo, J., Peng, H., Chen, M., Fu, Y.X., and Tang, H. (2020). PD-L1 on dendritic cells attenuates T cell activation and regulates response to immune checkpoint blockade. Nat. Commun. *11*, 4835. https://doi.org/10.1038/s41467-020-18570-x.
31. Mayoux, M., Roller, A., Pulko, V., Sammicheli, S., Chen, S., Sum, E., Jost, C., Fransen, M.F., Buser, R.B., Kowanetz, M., et al. (2020). Dendritic cells dictate responses to PD-L1 blockade cancer immunotherapy. Sci. Transl. Med. *12*, eaav7431. https://doi.org/10.1126/scitranslmed.aav7431.
32. Oh, S.A., Wu, D.C., Cheung, J., Navarro, A., Xiong, H., Cubas, R., Totpal, K., Chiu, H., Wu, Y., Comps-Agrar, L., et al. (2020). PD-L1 expression by dendritic cells is a key regulator of T-cell immunity in cancer. Nat. Cancer *1*, 681–691. https://doi.org/10.1038/s43018-020-0075-x.
33. Dammeijer, F., van Gulijk, M., Mulder, E.E., Lukkes, M., Klaase, L., van den Bosch, T., van Nimwegen, M., Lau, S.P., Latupeirissa, K., Schetters, S., et al. (2020). The PD-1/PD-L1-checkpoint restrains T cell immunity in tumor-draining lymph nodes. Cancer Cell *38*, 685–700.e8. https://doi.org/10.1016/j.ccell.2020.09.001.
34. Sugiura, D., Maruhashi, T., Okazaki, I.M., Shimizu, K., Maeda, T.K., Takemoto, T., and Okazaki, T. (2019). Restriction of PD-1 function by *cis*-PD-L1/CD80 interactions is required for optimal T cell responses. Science *364*, 558–566. https://doi.org/10.1126/science.aav7062.
35. Öhlund, D., Handly-Santana, A., Biffi, G., Elyada, E., Almeida, A.S., Ponz-Sarvise, M., Corbo, V., Oni, T.E., Hearn, S.A., Lee, E.J., et al. (2017). Distinct populations of inflammatory fibroblasts and myofibroblasts in pancreatic cancer. J. Exp. Med. *214*, 579–596. https://doi.org/10.1084/jem.20162024.
36. Elyada, E., Bolisetty, M., Laise, P., Flynn, W.F., Courtois, E.T., Burkhart, R.A., Teinor, J.A., Belleau, P., Biffi, G., Lucito, M.S., et al. (2019). Cross-species single-cell analysis of pancreatic ductal adenocarcinoma reveals antigen-presenting cancer-associated fibroblasts. Cancer Discov. *9*, 1102–1123. https://doi.org/10.1158/2159-8290.CD-19-0094.
37. Mariathasan, S., Turley, S.J., Nickles, D., Castiglioni, A., Yuen, K., Wang, Y., Kadel, E.E., Koeppen, H., Astarita, J.L., Cubas, R., et al. (2018). TGFβ attenuates tumour response to PD-L1 blockade by contributing to exclusion of T cells. Nature *554*, 544–548. https://doi.org/10.1038/nature25501.
38. Thomas, D.A., and Massagué, J. (2005). TGF-beta directly targets cytotoxic T cell functions during tumor evasion of immune surveillance. Cancer Cell *8*, 369–380. https://doi.org/10.1016/j.ccr.2005.10.012.
39. Wu, P., Geng, B., Chen, Q., Zhao, E., Liu, J., Sun, C., Zha, C., Shao, Y., You, B., Zhang, W., et al. (2020). Tumor cell-derived TGFβ1 attenuates antitumor immune activity of T cells via regulation of PD-1 mRNA. Cancer Immunol. Res. *8*, 1470–1484. https://doi.org/10.1158/2326-6066.CIR-20-0113.
40. Grauel, A.L., Nguyen, B., Ruddy, D., Laszewski, T., Schwartz, S., Chang, J., Chen, J., Piquet, M., Pelletier, M., Yan, Z., et al. (2020). TGFβ-blockade uncovers stromal plasticity in tumors by revealing the existence of a subset of interferon-licensed fibroblasts. Nat. Commun. *11*, 6315. https://doi.org/10.1038/s41467-020-19920-5.
41. Ciardiello, D., Elez, E., Tabernero, J., and Seoane, J. (2020). Clinical development of therapies targeting TGFβ: current knowledge and future perspectives. Ann. Oncol. *31*, 1336–1349. https://doi.org/10.1016/j.annonc.2020.07.009.
42. Lind, H., Gameiro, S.R., Jochems, C., Donahue, R.N., Strauss, J., Gulley, J.L., Palena, C., and Schlom, J. (2020). Dual targeting of TGF-β and PD-L1 via a bifunctional anti-PD-L1/TGF-βRII agent: status of preclinical and clinical advances. J. Immunother. Cancer *8*, e000433. https://doi.org/10.1136/jitc-2019-000433.
43. Yoo, C., Oh, D.Y., Choi, H.J., Kudo, M., Ueno, M., Kondo, S., Chen, L.T., Osada, M., Helwig, C., Dussault, I., and Ikeda, M. (2020). Phase I study of bintrafusp alfa, a bifunctional fusion protein targeting TGF-β and PD-L1, in patients with pretreated biliary tract cancer. J. Immunother. Cancer *8*, e000564. https://doi.org/10.1136/jitc-2020-000564.
44. Stuart, T., Butler, A., Hoffman, P., Hafemeister, C., Papalexi, E., Mauck, W.M., Hao, Y., Stoeckius, M., Smibert, P., and Satija, R. (2019). Comprehensive integration of single-cell data. Cell *177*, 1888–1902.e21. https://doi.org/10.1016/j.cell.2019.05.031.
45. Franzén, O., Gan, L.M., and Björkegren, J.L.M. (2019). PanglaoDB: a web server for exploration of mouse and human single-cell RNA sequencing data. Database *2019*, baz046. https://doi.org/10.1093/database/baz046.
46. Huang, d.W., Sherman, B.T., and Lempicki, R.A. (2009). Systematic and integrative analysis of large gene lists using DAVID bioinformatics resources. Nat. Protoc. *4*, 44–57. https://doi.org/10.1038/nprot.2008.211.
47. Huang, d.W., Sherman, B.T., and Lempicki, R.A. (2009). Bioinformatics enrichment tools: paths toward the comprehensive functional analysis of large gene lists. Nucleic Acids Res. *37*, 1–13. https://doi.org/10.1093/nar/gkn923.
48. Khomtchouk, B.B., Hennessy, J.R., and Wahlestedt, C. (2017). shinyheatmap: ultra fast low memory heatmap web interface for big data genomics. PLoS One *12*, e0176334. https://doi.org/10.1371/journal.pone.0176334.
49. Trapnell, C., Cacchiarelli, D., Grimsby, J., Pokharel, P., Li, S., Morse, M., Lennon, N.J., Livak, K.J., Mikkelsen, T.S., and Rinn, J.L. (2014). The dynamics and regulators of cell fate decisions are revealed by pseudotemporal ordering of single cells. Nat. Biotechnol. *32*, 381–386. https://doi.org/10.1038/nbt.2859.
50. Hashimoto, M., Yamashita, Y., and Takemoto, T. (2016). Electroporation of Cas9 protein/sgRNA into early pronuclear zygotes generates non-mosaic mutants in the mouse. Dev. Biol. *418*, 1–9. https://doi.org/10.1016/j.ydbio.2016.07.017.

STAR★METHODS

KEY RESOURCES TABLE

REAGENT or RESOURCE	SOURCE	IDENTIFIER
Antibodies		
Anti-mouse VEGF monoclonal antibody (B20–4.1.1)	Genetech	N/A
Anti-mouse PD-L1 monoclonal antibody (6E11)	Genetech	N/A
Anti-PD-1 monoclonal antibody (RMP1-14)	BioXCell	Cat#BE0146; RRID:AB_10949053
Mouse IgG1 isotype control, unknown specificity	Bioxcell	Cat#BE0083; RRID:AB_1107784
Rat IgG2a isotype control, anti-trinitrophenol	Bioxcell	Cat#BE0089; RRID:AB_1107769
Anti-CD45 antibody coupled to magnetic beads	Miltenyi Biotech	Cat#130-052-301; RRID:AB_2877061
$CD8a^+$ T cell isolation kit	Miltenyi Biotech	Cat#130-104-075
PE-Cy7 conjugated anti-mouse CD45 antibody	eBioscience	Cat#25-0451-82; RRID:AB_2734986
FITC conjugated anti-mouse CD34 antibody	BD Pharmingen	Cat#553733; RRID:AB_395017
APC conjugated anti-mouse F4/80 antibody	BioLegend	Cat#123115; RRID:AB_893493
PE conjugated anti-human CD45 antibody	eBioscience	Cat#12-9459-42; RRID:AB_10718238
Rat anti-CD31/PECAM-1 monoclonal antibody	BD Pharmingen	Cat#550274; RRID:AB_393571
Rat anti-Gr-1 monoclonal antibody	BD Pharmingen	Cat#550291; RRID:AB_393586
Rat anti-CD8a monoclonal antibody	BD Pharmingen	Cat#550281; RRID:AB_2275792
Rabbit anti-COL1A1 polyclonal antibody	Abcam	Cat#ab21286; RRID:AB_446161
Rat anti-CD45 monoclonal antibody	BD Pharmingen	Cat#553076; RRID:AB_394606
Rabbit anti-Foxp3 polyclonal antibody	Novus Biologicals	Cat#NB600-245; RRID:AB_10001076
Rabbit anti-alpha smooth muscle actin monoclonal antibody	Abcam	Cat#ab124964; RRID:AB_11129103
Alexa 488-labeled secondary antibody	Invitrogen	Cat#A11008; RRID:AB_143165
Alexa 594-labeled secondary antibody	Invitrogen	Cat#A11007; RRID:AB_10561522
Rabbit anti-Ki67polyclonal antibody	Abcam	Cat#ab15580; RRID:AB_443209
Rabbit anti-FSP-1 monoclonal antibody	Cell Signaling Technology	Cat#13018; RRID:AB_2750896
PE conjugated anti-CD86 antibody	eBioscience	Cat#12-0862-81; RRID:AB_465767
Chemicals, peptides, and recombinant proteins		
SB525334	selleck	Cat#S1476
BSA	Sigma	Cat#A9418-5G
collagenase IV	Roche	Cat#17104019
DNase 1	Sigma	Cat#11284932001
Bovine fibronectin	R&D systems	Cat#1030-FN
ReadiDrop PI staining	Bio-Rad	Cat#1351101
OCT compound	Sakura Finetechnical Co.	Cat#4583
Hematoxylin	DAKO	Cat#S3309
Mitomycin C	Sigma	Cat#M4287
Recombinant mouse M-CSF	R&D Systems	Cat# 416-ML-010
Recombinant mouse GM-CSF	Peprotech	Cat#315-03
Recombinant mouse IL-4	Peprotech	Cat#214-14
Recombinant mouse TNF-α	Peprotech	Cat#315-01A
Recombinant mouse TGF-β	R&D Systems	Cat#7666-MB
Critical commercial assays		
RNeasy Mini Kit	Qiagen	Cat#74004
High-Capacity cDNA Reverse Transcription Kit	Applied Biosystems	Cat#4387406
SYBR® Premix Ex Taq™	Takara	Cat#RR820A

(*Continued on next page*)

Continued

REAGENT or RESOURCE	SOURCE	IDENTIFIER
Chromium Single-cell 3′ Reagent kit v3.1	10x Genomics	Cat#1000128
High Sensitivity DNA kit	Agilent	Cat#5067-4626
3,3′-diaminobenzidine tetrahydrochloride (DAB) Liquid System	DAKO	Cat#K3468
Fluoro-KEEPER Antifade Reagent, Non-Hardening Type with DAPI	Nacalai tesque	Cat#12745-74
CellTrace CFSE Cell Proliferation Kit	Thermo	Cat#C34554
96-well U-bottom plate	Corning	Cat#3799
Deposited data		
Raw and analyzed scRNA-seq data (mouse)	this paper	GEO: GSE223998
Raw and analyzed scRNA-seq data (human)	this paper	GEO: GSE223923
Experimental models: Cell lines		
AB1-HA	Public Health England	Cat#12070506
LLC	ATCC	Cat#CRL-1642^{TM}
Experimental models: Organisms/strains		
BALB/c	Charles River Japan Inc.	N/A
C57BL/6	Charles River Japan Inc.	N/A
BALB/c: CD86 KO: BALB/cAnNCrlj-*Cd86*^{tm1}	Setsurotech Inc.	N/A
BALB/c: CD80 KO: BALB/cAnNCrlj-*Cd80*^{tm1}	Setsurotech Inc.	N/A
Oligonucleotides		
Cd274 primer	Eurofins	(forward):TGTGGAGAAATGTGGCGTTG (reverse):CAGACCACAAGCTGCCAATC
Cd86 primer	Eurofins	(forward):CACGGACTTGAACAACCAGAC (reverse):CTCCACGGAAACAGCATCTGA
Adgre1 primer	Eurofins	(forward):AGCTCCCATTCCCAGACTTC (reverse):TGCCATCAACTCATGATACCCT
Acta2 primer	Eurofins	(forward):TGGAGAAGCCCAGCCAGTCG (reverse):ACATAGCTGGAGCAGCGTCT
Col1a1 primer	Eurofins	(forward):CGCAAAGAGTCTACATGTCT (reverse):TTAGGCCATTGTGTATGCAG
Cd45 primer	Eurofins	(forward):AGTGCAAAGGAGACCCTATT (reverse):ATCACTGGGTGTAGGTGTTT
Rps29 primer	Eurofins	(forward):TCTGAAGGCAAGATGGGTCA (reverse):CATTCAAGGTCGCTTAGTCC
Software and algorithms		
2100 Expert version B.02.07.SI532 software program	Agilent	N/A
DNBSEQ-G400 PE150 platform	MGI Tech Japan	N/A
CellRanger	10x Genomics	https://www.10xgenomics.com/
Seurat, R package, version 3.1.5	Stuart et al.[44]	https://satijalab.org/seurat/
PanglaoDB database	Franzén et al.[45]	https://panglaodb.se/
DAVID webtool (david.ncifcrf.gov)	Huang et al.[46,47]	https://david.ncifcrf.gov/
wPGSA webtool	Kawakami et al.[23]	http://wpgsa.org/
shinyheatmap webtool	Khomtchouk et al.[48]	http://shinyheatmap.com/
Monocle 2	Trapnell et al.[49]	http://cole-trapnell-lab.github.io/monocle-release/
ImageJ software program	National Institutes of Health	https://imagej.nih.gov/ij/
FlowJo software program	Treestar Inc	https://www.flowjo.com/
Other		
2100 Bioanalyzer	Agilent	Cat#G2939BA
Auto MACS instrument	Miltenyi Biotech	Cat#130-092-545

(*Continued on next page*)

Continued

REAGENT or RESOURCE	SOURCE	IDENTIFIER
LE-SH800BC	Sony	N/A
CFX96 real-time PCR system™	Takara	Cat#184-5096J1
BZ-9000 microscope	Keyence	N/A
BX61 fluorescence light microscope	Olympus	N/A
BD LSRFortessa	BD Bioscience	N/A

RESOURCE AVAILABILITY

Lead contact

Further information and requests for resources and reagents should be directed to and will be fulfilled by the lead contact, Yasuhiko Nishioka (yasuhiko@tokushima-u.ac.jp).

Materials availability

All unique/stable reagents generated in this study are available from the lead contact without restriction.

Data and code availability

Single-cell RNA-seq data have been deposited at GEO and are publicly available as of the date of publication. Accession numbers are listed in the key resources table. Microscopy data reported in this paper will be shared by the lead contact upon request.

This paper does not report original code.

Any additional information required to reanalyze the data reported in this paper is available from the lead contact upon request.

EXPERIMENTAL MODEL AND SUBJECT DETAILS

Cell lines

The mouse MPM cell line AB1-HA, a transfectant with the gene encoding influenza HA into AB1 cells, was purchased from Public Health England (London, UK). The mouse lung cancer cell line Lewis lung carcinoma (LLC), was purchased from ATCC (Manassas, VA, USA). AB1-HA was maintained in DMEM supplemented with 10% heat-inactivated fetal bovine serum (FBS), penicillin (100 U ml^{-1}) and streptomycin (50 $\mu g\ mL^{-1}$). LLC was maintained in RPMI 1640 medium supplemented with 10% FBS, penicillin (100 U ml^{-1}) and streptomycin (50 $\mu g\ mL^{-1}$). All cells were cultured at 37°C in a humidified atmosphere of 5% CO_2 in air.

Animals

Six-week-old male BALB/c mice and C57BL/6 mice were obtained from Charles River Japan Inc. (Shiga, Japan). CD86 KO mice and CD80 KO mice were generated by Setsurotech Inc. (Tokushima, Japan) with a genome editing technique.[50] Briefly, *in vitro* fertilized zygotes (BALB/c × BALB/c) were electroporated with 100 ng μL^{-1} Cas9 protein, 100 ng μL^{-1} crRNAs, and 100 ng μL^{-1} tracrRNA. Two crRNAs targeting upstream and downstream of the CD86 or CD80 gene were used. We designed the target sequences of crRNAs as follows: CD86 crRNA1 (5′-CTTTTTAAACTCCAGCACCA-3′), CD86 crRNA2 (5′ -GTGACAGTCTTGCTGATCTC-3′), CD80 ex2 crRNA1 (5′- TACCTTATCTTTCACTGACTTGG-3′), CD80 ex3 crRNA2 (5′- ATGTTGCTTACGTTTTTCCCAGG-3′). Electroporated zygotes were transferred into the oviduct of pseudopregnant female mice, and the mutant mice were born on E19. Mice were maintained under specific-pathogen-free conditions throughout this study. All experiments were performed in accordance with the guidelines established by the Tokushima University Committee on Animal Care and Use. At the end of each *in vivo* experiment, mice were anesthetized with isoflurane and euthanized humanely by cutting the subclavian artery. All experimental protocols were reviewed and approved by the animal research committee of The University of Tokushima, Japan (approved number T30-130).

Clinical sample

Surgically resected tumor tissue from four lung adenocarcinoma patients were used in the present study to isolate the tumor-infiltrating immune cells. Informed consent was obtained from all patients, and the protocol was approved by the institutional review board of Tokushima University Hospital (approved number 3882). Clinical characteristics of cases used in this study were shown in Figure S4.

METHOD DETAILS

Reagents

Anti-mouse VEGF monoclonal antibody (B20–4.1.1) and anti-mouse PD-L1 monoclonal antibody (6E11) were kindly provided by Genetech (South San Francisco, CA, USA). Anti-PD-1 monoclonal antibody (RMP1-14) and Isotype control IgG (mouse IgG1, rat

IgG2a) were purchased from BioXCell (West Lebanon, NH, USA). For *in vivo* studies, the neutralizing antibodies were diluted in phosphate-buffered saline (PBS). TGF-β/SMAD signal inhibitor, SB525334 was purchased form Selleck Chemicals (Houston, TX, USA).

Animal experiments

AB1-HA cells (1.0×10^6 cells per mouse) suspended in 0.1 mL PBS were subcutaneously inoculated to the right flank of BALB/c mice. LLC cells (1.0×10^6 cells per mouse) were subcutaneously inoculated to C57BL/6 mice. The tumor size was measured twice a week using vernier calipers, where volume = $ab^2\,2^{-1}$ (a, long diameter; b, short diameter). To determine the effect of PD-1/PD-L1 and VEGF blockade on tumor growth, mice were treated twice a week with anti-PD-L1 antibody (0.5 mg kg^{-1} per mouse), anti-PD-1 antibody (200 μg per mouse) and anti-VEGF antibody (0.5 or 1 or 5 mg kg^{-1} per mouse) or isotype control IgG by intraperitoneal injection from day 7, until they became moribund. The mice were killed humanely, and the tumors were resected for further analyses on day 21. To examine the effect of fibrocytes and macrophages on the antitumor effects of PD-1/PD-L1 blockade, mouse lung fibrocytes or bone marrow-derived macrophages (2.0×10^5 cells per mouse, suspended in 100 μL PBS) were implanted adjacent to the surface of subcutaneous tumor tissue twice a week from day 7. For the control group, we injected 100 μL PBS. To examine the effects of TGF-β/SMAD signal inhibitor, SB525334 (10 mg per kg per mouse, orally) was administered from day 7. For oral administration, SB525334 diluted in 30% propylene glycol, 5% dimethyl sulfoxide, and 65% D5W (dextrose 5% in water).

Purification of mouse lung fibrocytes

Mouse fibrocytes were isolated according to previously published methods.[16,18] Mouse lungs removed from BALB/c mice were minced with scissors and incubated with DMEM including 1 mg mL^{-1} BSA (Sigma, St Louis, MO), 1 mg mL^{-1} collagenase IV (Roche, Basel, Switzerland) and 100 μg mL^{-1} DNase 1 (Sigma) for 1 h at 37°C. Single cell suspensions from whole lungs were incubated in DMEM supplemented with 20% FBS in 200-mm fibronectin-coated dishes. After seven days, trypsinized cells were incubated with anti-CD45 antibody coupled to magnetic beads (Miltenyi Biotech, Auburn, CA) for 15 min on ice. Labeled cells were separated into $CD45^+$ (fibrocytes) and $CD45^-$ (fibroblasts) populations using an Auto MACS instrument (Miltenyi Biotech) according to the manufacturer's instructions.

Purification of mouse macrophages

Murine bone marrow cells were obtained from the femur and tibia of seven-week-old BALB/c mice. To generate murine macrophages, bone marrow cells were cultured with murine recombinant M-CSF (20 ng mL^{-1}, R&D Systems) for seven days.

Purification of tumor-infiltrating immune cells

The tumor tissues collected from AB1-HA tumor-bearing BALB/c mice or LLC-bearing C57BL/6 mice treated with anti-VEGF antibody (5 mg kg^{-1}) were minced and suspended to provide single cells on day 21 after inoculation, as described above. The number of whole cells was counted using a hemocytometer, and 1×10^7 suspended cells were labeled with PE-Cy7 conjugated anti-mouse CD45 antibody (1:100 dilution, 30-F11, eBioscience, San Diego, CA, USA), FITC conjugated anti-mouse CD34 antibody (1:100 dilution, MEC 13.3; BD Pharmingen, Franklin Lakes, NJ, USA), and APC conjugated anti-mouse F4/80 antibody (1:100 dilution, BM8, BioLegend, San Diego, CA, USA). Dead cells were removed by ReadiDrop PI staining (Bio-Rad, Hercules, CA, USA). Tumor-infiltrating fibrocytes ($CD45^+CD34^+$ cells) and macrophages ($CD45^+F4/80^+CD34^-$ cells) were sorted by LE-SH800BC (Sony, Tokyo, Japan). The numbers of fibrocytes and macrophages were counted using a hemocytometer, and total RNA was extracted. Tumor-infiltrating APCs (5.0×10^4 cells per well) were seeded in 24-well plates and incubated with 10% FBS DMEM with or without mouse TGF-β (10 ng mL^{-1}, R&D Systems). After incubation for seven days, total RNA was extracted. Tumor-infiltrating immune cells were also isolated from clinical lung adenocarcinoma patients. The tumor tissues surgically resected from lung adenocarcinoma patients were minced with scissors and incubated with RPMI including 1 mg mL^{-1} BSA (Sigma), 1 mg mL^{-1} collagenase A (Roche) and 10 U ml^{-1} DNase 1 (Sigma) for 45 min at 37°C. The number of whole cells was counted using a hemocytometer, and the suspended cells were labeled with PE conjugated anti-human CD45 antibody (1:100 dilution, 2D1, Invitrogen, Carlsbad, CA, USA). Dead cells were removed by ReadiDrop PI staining (Bio-Rad). Tumor-infiltrating $CD45^+$ immune cells were sorted by LE-SH800BC (Sony).

Purification of bone marrow-derived dendritic cells

Mouse bone marrow cells (4×10^6 per well) were cultured in 6-well plates in 4 mL of RPMI 1640 supplemented with 10% heat-inactivated fetal calf serum, GM-CSF (20 ng mL^{-1}, Peprotech, Cranbury, NJ, USA), and IL-4 (20 ng mL^{-1}, Peprotech). The medium was removed on day 5 and new medium supplemented with GM-CSF (20 ng mL^{-1}, Peprotech), IL-4 (20 ng mL^{-1}, Peprotech), and TNF-α (20 ng mL^{-1}, Peprotech) was added. On day 7, non-adherent cells in the culture supernatant and loosely adherent cells were harvested by gentle washing and used as dendritic cells.

In vivo tracking of fibrocytes and dendritic cells

Mouse lung fibrocytes and bone marrow-derived dendritic cells were labeled by CFSE as described above. CFSE-labeled APCs (1.0×10^6 cells per mouse) were peritumorally transplanted to AB1-HA tumor bearing mice. Two days later, tumor tissue, and axillary and subiliac lymph nodes were collected and suspended to provide single cells. The number of tissue infiltrating-$CFSE^+$ cells was examined by flow cytometry.

qRT-PCR

Total RNA was extracted from tumor-infiltrating fibrocytes and macrophages using an RNeasy Mini Kit (Qiagen, Hilden, Germany) and reverse-transcribed to cDNA using a High-Capacity cDNA Reverse Transcription Kit (Applied Biosystems, Carlsbad, CA, USA) according to the manufacturer's instructions. RT-PCR was performed using a CFX96 real-time PCR system™ (BioRad, Hercules, CA, USA) or SYBR® Premix Ex Taq™ (TAKARA, Kyoto, Japan). Mouse *RPS29* mRNA was used as a housekeeping gene, and quantification was performed using the ΔΔCt method. The specific PCR primer pairs used for each studied gene were Cd274 (forward): 5′-TGTGGAGAAATGTGGCGTTG-3′; Cd274 (reverse): 5′-CAGACCACAAGCTGCCAATC-3′; Cd86 (forward): 5′-CACGGACTTGAACAACCAGAC-3′; Cd86 (reverse): 5′-CTCCACGGAAACAGCATCTGA-3′; Adgre1 (forward): 5′-AGCTCCCATTCCCAGACTTC-3′; Adgre1 (reverse): 5′-TGCCATCAACTCATGATACCCT-3′; Acta2 (forward): 5′-TGGAGAAGCCCAGCCAGTCG-3′; Acta2 (reverse): 5′-ACATAGCTGGAGCAGCGTCT-3′; Col1a1 (forward): 5′-CGCAAAGAGTCTACATGTCT-3′; Col1a1 (reverse): 5′-TTAGGCCATTGTGTATGCAG-3′; Cd45 (forward): 5′-AGTGCAAAGGAGACCCTATT-3′; Cd45 (reverse): 5′-ATCACTGGGTGTAGGTGTTT-3′; RPS29 (forward): 5′-TCTGAAGGCAAGATGGGTCA-3′; RPS29 (reverse): 5′-CATTCAAGGTCGCTTAGTCC-3′.

Single-cell RNA sequencing

$CD45^+$ tumor-infiltrating immune cells from AB1-HA-bearing mice and human lung adenocarcinoma patients were loaded on a Chromium 10x Instrument (10x Genomics, Pleasanton, CA, USA) to generate single-cell gel beads in emulsion. ScRNA-seq libraries were prepared using the Chromium Single-cell 3′ Reagent kit v3.1 (10x Genomics) according to the manufacturer's protocol. The quality of libraries was determined using an Agilent 2100 Bioanalyzer with the 2100 Expert version B.02.07.SI532 software program and a High Sensitivity DNA kit (Agilent, Santa Clara, CA, USA). Libraries were sequenced on a DNBSEQ-G400 PE150 platform (MGI Tech Japan, Tokyo, Japan), followed by computational alignment using CellRanger (version 3.0.2, 10x Genomics). Datasets were analyzed for quality control using Seurat (R package, version 3.1.5), that included selecting cells with a library complexity of more than 200 features.[44] Doublets and cells with high percentages of mitochondrial genes (>20%) were removed. A principal component analysis was performed using Seurat's RunPCA function, and the first seven principal components were used for cell clustering (resolution = 0.3) and UMAP dimensional reduction. The cluster markers were detected using Seurat's FindMarkers function, and cell types were annotated based on the cluster markers from the PanglaoDB database.[45] Mouse tumor-infiltrating fibrocytes (cluster 5) were analyzed for further sub-clustering. Scaling, a principal component analysis, clustering and UMAP dimensional reduction were performed as described above. Differentially expressed genes (DEGs) were investigated in each fibrocyte sub-cluster using Seurat's FindMarkers function. DEGs were filtered based on a >2-fold change and a maximum p value of 0.01. A GO analysis was conducted using the DAVID webtool (david.ncifcrf.gov) in order to investigate the functions of the DEGs.[46,47] A pseudotime analysis was performed using Monocle 2.[48] Responsible transcription regulators of fibrocytes, M1-like macrophages, and M2-like macrophages were predicted using the wPGSA webtool.[23] LogFC values of the top 100 DEGs of each cluster were loaded into a wPGSA analysis, and enrichment scores were calculated. A clustermap was created based on the enrichment score of 412 TFs in each cluster using the shinyheatmap webtool.[49]

Immunohistochemical studies

Excised tumor tissues from model mice were placed into OCT compound (Sakura Finetechnical Co., Tokyo, Japan) and snap-frozen. Frozen tissue sections (thickness: 8 μm) of tumors were fixed with 4% paraformaldehyde solution in PBS. To detect endothelial cells, rat anti-CD31/PECAM-1 monoclonal antibody (1:100 dilution, MEC 13.3; BD Pharmingen) was used. Appropriate secondary antibodies conjugated with peroxidase (ready to use, Nichirei, Tokyo, Japan) and the 3,3′-diaminobenzidine tetrahydrochloride (DAB) Liquid System (DAKO, Carpinteria, CA, USA) were used for immunostaining. Nuclei were counter-stained with hematoxylin (DAKO). The number of $CD31^+$ vessel structures per field was evaluated at ×200 magnification. Images were acquired using a Keyence BZ-9000 microscope (Keyence, Tokyo, Japan).

Immunofluorescence staining

Frozen tissue sections (thickness: 8 μm) were fixed with 4% paraformaldehyde solution in PBS and used for the identification of $CD8^+$ T cells using a rat anti-CD8a monoclonal antibody (1:150 dilution, 53-6.7; BD Pharmingen). To detect fibrocytes, a rabbit anti-COL1A1 polyclonal antibody (1:100 dilution, Abcam, Cambridge, MA) and rat anti-CD45 monoclonal antibody (1:50 dilution, 30-F11, BD Pharmingen) were used. To identify MDSCs, a rat anti-Gr-1 monoclonal antibody (1:50 dilution, RB6-8C5, BD Pharmingen) was used. To detect T_{regs}, a rabbit anti-Foxp3 polyclonal antibody (1:400 dilution, Novus Biologicals, Centennial, CO, USA) was used. To identify myofibroblast, a rabbit anti-alpha smooth muscle actin monoclonal antibody (1:150 dilution, EPR5368, Abcam) was used. Alexa 488-and Alexa 594-labeled secondary antibodies (1:250 dilution; Invitrogen) were used for immunofluorescent detection. Nuclei were counterstained with DAPI. In each slide, the number of positive cells was counted under a fluorescence microscope at × 200 magnification. Proliferating $CD8^+$ T cells were determined by double staining for CD8 and Ki67 (rabbit polyclonal antibody, 1:1000 dilution, Abcam). The colocalization of fibrocytes and $CD8^+$ T cells were examined by double staining for CD8 and FSP-1 (1:100 dilution, D9F9D, Cell Signaling Technology, Danvers, MA, USA). These images were acquired using an Olympus BX61 fluorescence light microscope (Olympus, Tokyo, Japan) and Keyence BZ-9000 microscope (Keyence). The αSMA-positive areas were calculated using the ImageJ software program (National Institutes of Health, Bethesda, MD, USA).

Flow cytometry

To examine the surface expression of CD86 in mouse lung or AB1-HA tumor-derived fibrocytes, PE conjugated antibodies to CD86 (1:50, GL-1, eBioscience) were used. The percentage of tumor-infiltrating fibrocytes ($CD45^+CD34^+$ cells) and FC3 ($CD45^+CD34^+$ $CD86^+$ cells) were examined in AB1-HA tumor tissue treated with anti-VEGF antibody (5 mg kg^{-1} per mouse) or control IgG. The stained cells were analyzed by flow cytometry using a BD LSRFortessa (BD Bioscience) for acquisition and the FlowJo software program (Treestar Inc, Ashland, OR) for the analysis.

Proliferation assay of $CD8^+$ T cells

In murine allogenic MLR, $CD8^+$ splenic T cells were harvested from C57BL/6 mice with a $CD8a^+$ T cell isolation kit, as described (no. 130-104-075; Miltenyi Biotec). $CD8a^+$ T cells were labeled with a CellTrace CFSE Cell Proliferation Kit (Thermo, Waltham, MA, USA). Cells were incubated with CFSE-dye (5 μM) at 37°C for 20 min, and then incubated with 10% FBS DMEM at 37°C for 5 min. Tumor-infiltrating fibrocytes or macrophages were treated with mitomycin C (25 mg mL^{-1}, Sigma) at 37°C for 30 min. CFSE-labeled $CD8^+$ T cells (2×10^5 cells per well) were stimulated with tumor-infiltrating fibrocytes or macrophages from BALB/c mice (1×10^3–2×10^4 cells per well) for 96 h in a 96-well U-bottom plate (Corning, NY, USA). T cell proliferation was determined as the percentage of $CFSE^{low}$ cells by flow cytometry. To investigate the effect of anit-PD-L1 antibody, $CD8^+$ splenic T cells (2×10^5 cells per well) were stimulated with tumor-infiltrating APCs (2×10^3 cells per well) with or without anti-PD-L1 antibody (20 μg mL^{-1}, Bioxcell).

QUANTIFICATION AND STATISTICAL ANALYSIS

The data are presented as the mean ± standard error of the mean. The statistical analyses were performed using Student's t-test for unpaired samples, the Mann-Whitney-*U* test or a one-way analysis of variance, followed by Tukey's multiple-comparison post-hoc test, as appropriate. p values of <0.05 were considered to indicate statistical significance.